



Geochemistry, Geophysics, Geosystems



RESEARCH ARTICLE

10.1029/2023GC010981

Key Points:

- We explore how the silica metasomatism of serpentinized peridotite beneath Guerrero, Mexico, can produce talc-rich rocks
- Talc is predicted to grow in serpentinite where subducting basalts experience metamorphic dehydration
- Local advection of silica cannot produce geophysically observable talc volumes but will still produce thin zones of talc-rich rocks

Supporting Information:

Supporting Information may be found in the online version of this article.

Correspondence to:

P. C. Lindquist, plindqui@uw.edu

Citation:

Lindquist, P. C., Condit, C. B., Hoover, W. F., Hernández-Uribe, D., & Guevara, V. E. (2023). Metasomatism and slow slip: Talc production along the flat subduction plate interface beneath Mexico (Guerrero). *Geochemistry, Geophysics, Geosystems*, 24, e2023GC010981. https://doi.org/10.1029/2023GC010981

Received 4 APR 2023 Accepted 12 JUL 2023

© 2023 The Authors. Geochemistry, Geophysics, Geosystems published by Wiley Periodicals LLC on behalf of American Geophysical Union. This is an open access article under the terms of the Creative Commons Attribution License, which permits use, distribution and reproduction in any medium, provided the original work is properly cited.

Metasomatism and Slow Slip: Talc Production Along the Flat Subduction Plate Interface Beneath Mexico (Guerrero)

P. C. Lindquist¹, C. B. Condit¹, W. F. Hoover¹, D. Hernández-Uribe², and V. E. Guevara³

¹Department of Earth and Space Sciences, University of Washington, Seattle, WA, USA, ²Department of Earth and Environmental Sciences, University of Illinois Chicago, Chicago, IL, USA, ³Department of Geology, Amherst College, Amherst, MA, USA

Abstract Talc-rich rocks are common in exhumed subduction zone terranes and may explain geophysical observations of the subduction zone interface, particularly beneath Guerrero, Mexico, where the Cocos plate subducts horizontally beneath North America and episodic tremor and slow slip (ETS) occurs. We present petrologic models exploring (a) the degree of silica metasomatism required to produce talc in serpentinized peridotites at the pressure-temperature conditions of the plate interface beneath Guerrero and (b) the amount of silica-bearing water produced by rocks from the subducting Cocos plate and the location of fluid pulses. We estimate the volumes of talc produced by the advection of silica-rich fluids into serpentinized peridotites at the plate interface over the history of the flat-slab system. In the ETS-hosting region, serpentinites must achieve ~43 wt. % SiO₂ to stabilize talc, but minor additions of silica beyond this produce large volumes of talc. Our models of Cocos plate dehydration predict that water flux into the interface averages 3.9×10^4 kg m⁻² Myr⁻¹ but suggest that only where subducting basalts undergo major dehydration reactions will sufficient amounts of silica-rich fluids be produced to drive significant metasomatism. We suggest that talc produced by advective transport of aqueous silica alone cannot account for geophysical interpretations of km-thick zones of talc-rich rocks beneath Guerrero, although silica-bearing fluids that migrate along the plate interface may promote broader metasomatism. Regions of predicted talc production do, however, overlap with the spatial occurrence of ETS, consistent with models of slow slip based on the frictional deformation of metasomatic lithologies.

Plain Language Summary The subduction zone at Guerrero, Mexico, hosts poorly understood fault slip phenomena called episodic tremor and slow slip (ETS), and seismic studies of this subduction zone suggest that the deep interface between the Cocos plate and overriding North American plate contains rocks that are rich in the mineral talc. Talc is a weak mineral that can preferentially host deformation and may play a role in facilitating ETS in subduction zones. The presence of talc, however, requires chemical alteration of rocks at the plate interface, so we use Guerrero as a natural lab for exploring how talc might be produced in order to host ETS and produced the observed seismic signatures. We can use the thermodynamic properties of minerals to predict which minerals will occur in rocks that make up the mantle above the subducting Cocos plate, as well as when minerals in subducting rocks will break down to release water. This allows us to predict how much water will be released by the Cocos plate and subsequently how much talc can grow in the plate interface. Although the model for alteration we explore does not explain the geophysical observations at Guerrero, talc is still expected to be produced within regions that experience ETS.

1. Introduction

The interface between subducting and overriding plates in a subduction zone deforms by a complex suite of slip behaviors that include earthquakes, slow slip events (SSEs), tectonic tremor, and aseismic creeping. The mode of deformation in these fault zones is a consequence of a wide range of factors, including the composition of the plates (e.g., lithology and mineralogy), pressure, temperature, stress, and the presence and movement of fluids (e.g., Agard et al., 2018; Nishiyama et al., 2023; Tarling et al., 2019; Ujiie et al., 2022). However, the chemical processes that affect the composition and thus rheology of the plate interface in subduction zones remain understudied. For example, metasomatism can alter the strength of rocks prior to and during subduction by promoting the growth of weak mineral phases like chlorite and talc that, in turn, can localize deformation (Bebout & Barton, 2002; Gyomlai et al., 2021; Hernández-Uribe et al., 2020; Hirauchi et al., 2013). Such metasomatized rocks are common in exhumed paleo-subduction complexes worldwide (e.g., Codillo, Klein, Dragovic, et al., 2022; French & Condit, 2019; Hoover et al., 2022; Peacock & Hyndman, 1999).

LINDOUIST ET AL. 1 of 23

Talc $(Mg_3Si_4O_{10}(OH)_2)$ is a hydrous sheet silicate that occurs in metasomatic and metamorphic ultramafic and carbonate rocks, and is hypothesized to be rheologically significant in subduction zones (e.g., French & Condit, 2019; Peacock & Wang, 2021). During isochemical metamorphism, talc is not predicted to be stable at typical slab-top fluid saturated subduction zone conditions within major subducted lithologies (e.g., metabasalts, metasedimentary rocks), so talc is thought to be produced through the metasomatism—often hypothesized to form through the interaction of silica-rich fluids with rocks in the subduction zone (e.g., Manning, 1997). Experiments and modeling of the simple MgO-SiO₂-H₂O system indicate that talc is stable from the seafloor to a maximum temperature of $\sim 800^{\circ}$ C at 1–2 GPa, and a maximum pressure of 5 GPa at $\sim 700^{\circ}$ C (Pawley & Wood, 1995 and references therein). This wide range of stability of talc and the expected ubiquity of silica-rich fluids in the lithosphere is reflected by the common occurrence of talc in oceanic and continental fault zones (e.g., Boschi et al., 2006; Collettini et al., 2009; Moore & Rymer, 2007) and exhumed suites of subduction-related rocks (e.g., Bebout & Barton, 1993; French & Condit, 2019; Hirauchi et al., 2020; Hoover et al., 2022; Spandler et al., 2008). Subduction zones in which silica-saturated fluids released by the subducting slab interact with peridotite in the mantle wedge, are therefore a likely setting for the production of talc in rocks near the plate interface up to high pressures and temperatures.

Mechanically, talc has very low frictional strength (e.g., Moore & Lockner, 2008) and given its potential ubiquity along the plate interface in the forearc suggests it could accommodate deformation over a wide range of pressure and temperature conditions. Even at the highest temperatures at which deformation experiments on talc have been performed (875°C), regions of talc will develop narrow zones of localized shearing and slip in which sheets of talc delaminate and slide past each other (Escartín et al., 2008). At high pressures (0.5–1.5 GPa) as well, talc continues to exhibit frictional behavior, with thermal weakening and an increasing tendency to localize deformation with increasing temperature (Boneh et al., 2023). The experimentally determined rate-and-state frictional parameters of talc also suggest that talc could be a material that is capable of producing SSEs. Deformation experiments on samples of mixed antigorite and quartz gouge at 300–500°C showed that talc growth occurred during deformation and localized strain in the samples, even with low (<10 vol. %) quantities of talc (Hirauchi et al., 2013). Talc exhibits velocity-strengthening behavior but tends toward velocity-neutral behavior at low slip rates (Hirauchi et al., 2020) and increasing bulk shear strain (Misra et al., 2014). Rheological modeling by French and Condit (2019) indicates that at the high pore-fluid pressures predicted to occur at the plate interface, talc schists should preferentially accommodate slow slip strain rates, corroborated by microstructural observations of natural talc-bearing subduction interface rocks (e.g., Hoover et al., 2022).

Here, we model the production of talc along the flat slab subducting beneath Mexico, where observed slip behaviors include earthquakes, SSEs, and tectonic tremor, occurring episodically in the form of episodic tremor and slip (ETS) events. Through a combination of thermodynamic models of both (a) subducting Cocos plate oceanic lithosphere metamorphism and (b) metasomatic alteration of hydrated mantle peridotites, we show that silica-rich fluids produced by dehydration reactions in MORB may contribute to the occurrence of talc along the plate interface in the Guerrero, Mexico subduction zone. We show that over a duration of 10 million years, greater than 10 vol. % talc can be produced through silica advection at the plate interface near where large volumes of fluids are predicted to be produced by metamorphic dehydration reactions in the subducting Cocos plate. These results demonstrate the importance of incorporating metasomatism into our models of plate boundary slip processes and provide a possible chemical mechanism to produce some of the common occurrences of talc observed in exhumed terranes.

2. Geologic Setting

2.1. The Middle American Subduction Zone Near Guerrero

The subducting Cocos plate in the Middle American subduction zone near the state of Guerrero, Mexico has a unique flat slab geometry (Figure 1). The Cocos plate subducts beneath the North American plate at the Middle American trench at rates of \sim 60 mm/yr near Acapulco, Mexico (DeMets et al., 2010). Here, the plate descends beneath Mexico at a typical subduction dip angle before flattening and horizontally subducting beneath the continental lithosphere of North America (Pérez-Campos et al., 2008). Between 120 and 290 km from the trench, the top of the flat slab lies at \sim 40 km depth (Figure 1, Kim et al., 2010). Although the map extent of the flat slab segment of the Cocos plate extends beyond the borders of the state of Guerrero, we refer to this as the Guerrero segment to remain consistent with previous literature.

LINDOUIST ET AL. 2 of 23

1525/2027, 2023, 8, Downloaded from https://agupubs.onlinelibrary.wiley.com/doi/10.1029/2023GC010981, Wiley Online Library on [09/08/2023]. See the Terms and Conditions (https://onlinelibrary.wiley.com/terms

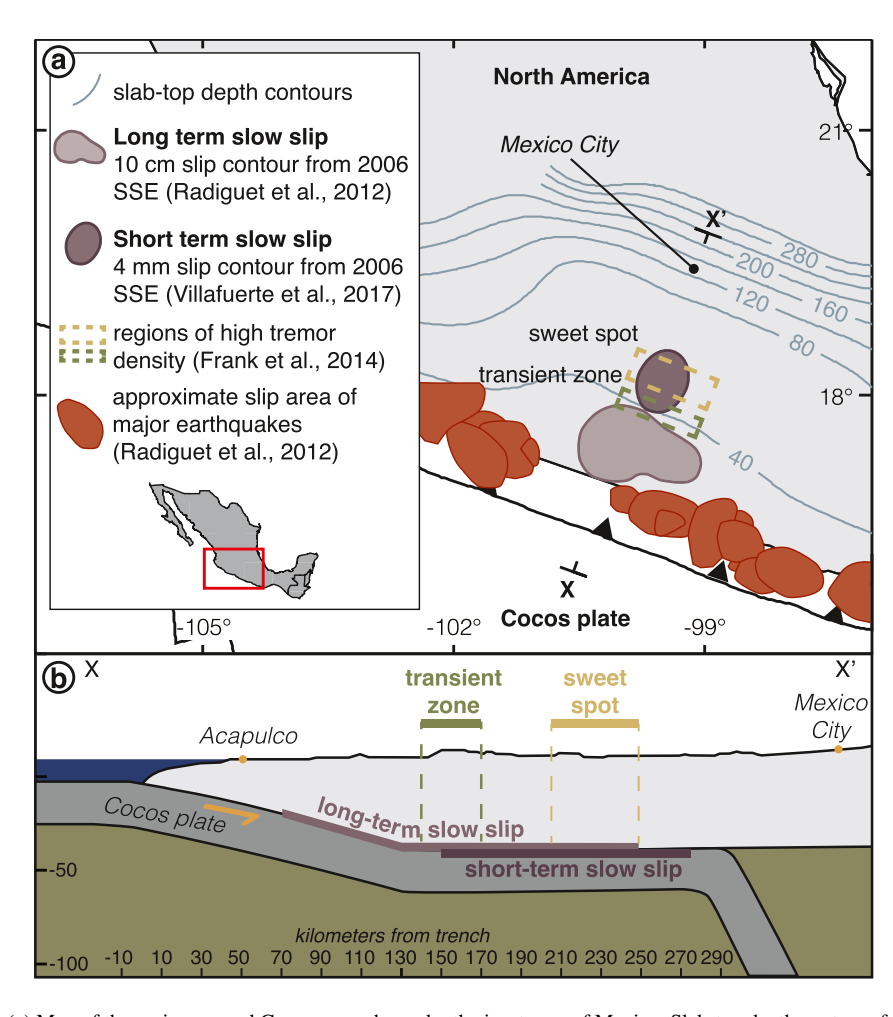


Figure 1. (a) Map of the region around Guerrero as shown by the inset map of Mexico. Slab-top depth contours from the Slab2 model (Hayes et al., 2018) show the extent of the flat slab region beneath Guerrero, Mexico, and locations of seismic events are outlined. (b) Schematic cross section of the flat slab subduction showing the distribution of tremor and slow slip on the flat plate interface.

Flat slab subduction initiated here around 16 Ma, and the flat portion reached its farthest landward extent around 10 Ma before beginning to roll back (Ferrari et al., 2012; Manea et al., 2013). This is evidenced by the migration of the volcanic front of the eastern Trans-Mexican Volcanic Belt between 16 and 9 Ma, and its continuing trenchward migration since 9 Ma. Between 20 and 10 Ma, Cocos–North American plate convergence rates near Guerrero were >100 mm/yr, with a significant component of margin-parallel motion. Since \sim 10 Ma, the convergence rate decreased to the modern, nearly margin-perpendicular rate of \sim 60 mm/yr for the last \sim 5 Myr (Sdrolias & Müller, 2006).

The Cocos plate is produced by fast spreading rates at the East Pacific Rise. Spreading rates at the East Pacific Rise where it produces the Cocos plate are relatively fast, ranging from 72 to 128 mm/yr (DeMets et al., 2010). The age of the subducting oceanic lithosphere at the Middle American trench near Guerrero is ~15 Ma (Manea et al., 2013). The composition of the Cocos plate has been investigated through limited seafloor drilling. Off the coast of Acapulco and 10 km seaward of the trench, hole 487 from leg 66 of the Deep Sea Drilling Project drilled through 171 m of sediment before striking basalt and an additional 7 m of basalt was recovered (Watkins et al., 1982). The sediments themselves consisted of 105.5 m of muddy silt atop 65.5 m of brown pelagic clay.

The thermal model of Manea and Manea (2011) provides an estimate of the present-day steady-state, 2D thermal structure of the subduction zone at Guerrero, using the slab geometry determined by the Meso-American Subduction Experiment. In their model, the top of the slab in the flat segment experiences isobaric heating from 350 to 650°C between 130 and 290 km from the trench at a depth of 40 km. We used this thermal model for investigating

LINDQUIST ET AL. 3 of 23

/agupubs.onlinelibrary.wiley.com/doi/10.1029/2023GC010981, Wiley Online Library on [09/08/2023]. See the Terms

thermally mediated processes at Guerrero because it uses precise plate geometries and age parameters for this location, compared to the thermal models developed by Syracuse et al. (2010) and van Keken et al. (2018), which average the subducting plate geometry over several hundred kilometers. We use the Manea and Manea (2011) model to determine the pressure-temperature (*P-T*) parameters to input into our petrologic models, and to determine the temperatures at which the various slip phenomena occur beneath Guerrero by pairing the thermal model with reported spatial distributions of slow slip and tremor events (e.g., Figure 2).

2.2. Geophysical Observations of the Plate Interface and Slip Behaviors

At the modern Guerrero subduction zone, seismic data suggest the presence of a 3–5 km thick low seismic velocity layer above the oceanic crust of the subducting Cocos plate, separating it from the continental crust of the overriding North America plate (Kim et al., 2010; Song et al., 2009). Song et al. (2009) report that an ultra-low velocity (S-wave velocities ~2–2.7 km/s) layer is present at the plate interface in the shallowly dipping to up-dip portion of the flat segment, which transitions to an uneven low velocity layer that extends from approximately 200 km from the trench to the down-dip end of the flat slab at 290 km. These low-velocity zones at the plate interface are suspected to represent mantle wedge material that was entrained during slab-flattening and has been serpentinized (Manea & Manea, 2011). Low Vp/Vs ratios and low Vs values suggest that this zone may contain significant quantities of talc (Kim et al., 2010), an interpretation supported by seismic anisotropy data, which has been further interpreted to represent an asymmetric shear fabric defined by deformed and aligned talc (Song & Kim, 2012).

Episodic tremor and slow slip have been regularly observed geodetically in Guerrero since 1998 (e.g., Lowry et al., 2001). The occurrence of ETS in this region is of particular interest because of the lack of $M_{\rm w} > 7.0$ subduction earthquakes in the ~100 km-wide northwestern part of the Guerrero seismic gap since 1911 (Figure 1a) (Kostoglodov et al., 2003). SSEs accommodate some of the relative motion between the Cocos and North American plates, likely affecting the earthquake cycle and increasing the recurrence interval for large earthquakes relative to adjacent regions on the Middle American subduction zone (Radiguet et al., 2012). SSEs have also been related to large earthquakes in the Guerrero and Oaxaca regions, potentially serving as a dynamic trigger for several $M_{\rm w} > 7.0$ earthquakes to the southeast of the Guerrero seismic gap by transferring stresses along the plate interface (Cruz-Atienza et al., 2021).

At Guerrero, the character of SSEs and associated tremor varies down-dip along the subduction interface (Figure 1). Two distinct regions of tectonic tremor activity have been described, known as the sweet spot and the transient zone, respectively (Frank et al., 2014; Husker et al., 2012; Kostoglodov et al., 2010). The sweet spot is located 205-250 km from the trench and is characterized by near-continuous tremor activity, whereas the transient zone is located 140-170 km from the trench and exhibits tremor activity primarily during SSEs (Frank et al., 2014; Husker et al., 2012). Two types of SSEs also occur along the subduction interface and overlap with these tremor-producing regions: short-term and long-term SSEs. Short-term SSEs occur exclusively on the flat segment of the subduction interface, between 150 and 275 km from the trench, with a ~3-month periodicity and equivalent moment magnitude of ~6.4 (e.g., Frank et al., 2015a, 2015b; Villafuerte & Cruz-Atienza, 2017). Long-term SSEs occur along the up-dip portions of the flat and shallowly dipping subduction interface between 70 and 250 km from the trench, recur every ~4 years, and have equivalent moment magnitudes of ~7.5 (e.g., Perez-Silva et al., 2021; Radiguet et al., 2012). Long-term SSEs are also spatially correlated with the observed low seismic velocity layer and local seismic anisotropy, suggesting that talc, which may be responsible for this region's unique seismic structure, may also facilitate SSEs (Song & Kim, 2012; Song et al., 2009). However, unless the rocks at the plate interface are chemically altered through silica metasomatism, it is unlikely that volumetrically significant talc will occur in this zone. We investigate the potential role of silica metasomatism in producing talc in this zone.

3. Mechanisms of Talc Production

The presence of talc beneath Guerrero was suggested by Kim et al. (2010) to be the result of silica metasomatism of mantle wedge rocks that were entrained during the flattening of the Cocos plate before 10 Ma. Silica metasomatism is one of several mechanisms for producing talc at the slab—mantle interface. This particular pathway involves the reaction of Mg-rich minerals—serpentine in the case of hydrated ultramafic rocks and dolomite

LINDOUIST ET AL. 4 of 23

15252027, 2023, 8, Downloaded from https://agupubs.onlinelibrary.wiley.com/doi/10.1029/2023GC010981, Wiley Online Library on [09/08/2023]. See the Terms and Conditions (https://onlinelibrary.wiley.com/terms-and-conditions) on Wiley Online Library for rules of use; OA articles are governed by the applicable Creative Commons. Licensee

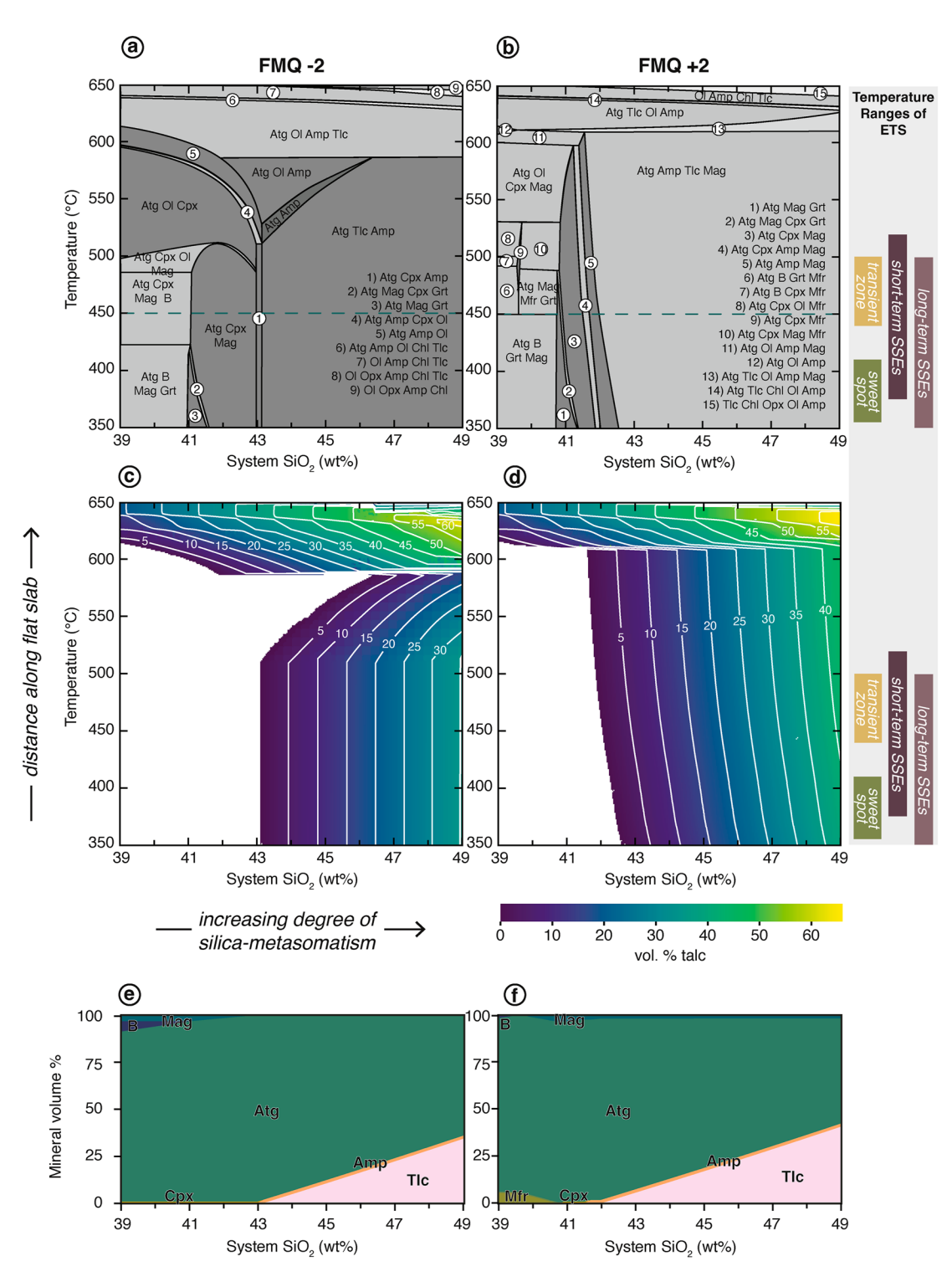


Figure 2. Silica metasomatism of serpentinized harzburgites at end-member redox conditions and 1.3 GPa and nominally water-saturated conditions. (a, b) Show equilibrium mineral assemblages at reduced and oxidized conditions, respectively. (c, d) Show the modal abundance of talc predicted by these reduced and oxidized models, respectively. Both oxidized and reduced models show that silica concentrations must reach ~43 wt. % to stabilize talc over the temperature range at which slow slip and tremor occur beneath Guerrero. (e, f) Show mineral modal abundance with increasing wt. % SiO₂ at 450°C—dashed line in (a, b)—in the reduced and oxidized models, respectively. Mineral abbreviations after Whitney and Evans (2010).

LINDQUIST ET AL. 5 of 23

online library. wiley. com/doi/10.1029/2023GC010981, Wiley Online Library on [09/08/2023]. See the Terms and Conditions

in the case of carbonate rocks—with silica-bearing fluids (e.g., Collettini et al., 2009; Manning, 1995). These processes produce talc by effectively increasing the amount of SiO₂ relative to MgO in the rock; therefore, metasomatic processes that also remove Mg from the rock may also promote talc production by passive Si enrichment. Other ways to produce talc include the addition of CO₂-rich fluids to serpentinite (e.g., Okamoto et al., 2021; Sieber et al., 2022; Spandler et al., 2008). The physical mechanism for the mass transfer involved in each of these may also be achieved through advection of elements in a fluid or diffusion between adjacent lithologies. New hybrid lithologies may also be produced through the physical mixing of various (potentially silica-rich) lithologies that are juxtaposed at the subduction interface (e.g., Hoover et al., 2022; Penniston-Dorland et al., 2014). Other studies of serpentinite metasomatism have employed reactive fluid flow models to predict the production of metasomatic minerals (e.g., Beinlich et al., 2020; Codillo, Klein, & Marschall, 2022). Codillo, Klein, and Marschall (2022) suggest that talc will not be a significant metasomatic product in subduction zones based on results of reactive transport modeling, but this is in contrast with geologic studies that indicate talc formation by silica metasomatism (e.g., Bebout & Barton, 1993; Hirauchi et al., 2020). Rather than focusing on fluid compositions, our models simulate the alteration of rock compositions through advective silica transport specifically by focusing on the equilibrium mineralogy of varying bulk-rock compositions.

4. Petrologic Modeling

To model chemical alteration of hydrated oceanic lithosphere entrained between the two plates along the flat slab, we created two coupled thermodynamic models of silica metasomatism, one focused on the amount of silica addition needed to create talc in hydrated mantle peridotites, and a second exploring the fluid and silica fluxes that are predicted from the subducting Cocos plate sediments and the hydrated top of the oceanic slab.

4.1. Modeling Approach

We model the equilibrium mineral assemblages of metasomatized serpentinite and subducting metasedimentary and basaltic rocks using the Gibbs free energy minimization software Perple_X 6.9.0 (Connolly & Petrini, 2002). To explore the silica metasomatism of hydrated peridotites, we created temperature-composition (T-X models) pseudosections at a constant pressure of 1.3 GPa—equivalent to \sim 40 km depth of the flat slab in the thermal model of Manea and Manea (2011)—and temperatures varying from 350 to 650°C, encompassing the range of temperatures estimated for the plate interface at Guerrero over this flat segment. We also simulate the isochemical metamorphism of metasedimentary and metabasalts over this same pressure-temperature (P-T) path. Modeled pressures and temperatures are based on estimates of conditions at the plate interface that are extracted from the thermal model of Manea and Manea (2011). From the phase-equilibrium models, we can also extract physical properties of the modeled rocks, such as density, based on the predicted mineral assemblages.

Serpentinized peridotites are modeled in the chemical system CaO-FeO-MgO-Al₂O₃-SiO₂-H₂O-O₂ (CFMASHO) using the ds55 thermodynamic database of Holland and Powell (1998) and fluid equation of state model of Holland and Powell (1991). Metasedimentary and basaltic rocks are modeled using the MnO-Na₂O-CaO- K₂O-FeO-MgO-Al₂O₃-SiO₂-H₂O-TiO₂ (MnNCKFMASHT) and Na₂O-CaO-FeO-MgO-Al₂O₃-SiO₂-H₂O-TiO₂ (NCFMASHT) systems, respectively, and the ds62 thermodynamic database of Holland and Powell (2011) and fluid equation of state model of Pitzer and Sterner (1994). The phase solution models used for each lithology are reported in Tables S1-S3 in Supporting Information S1. All models were run at water-saturated conditions to simulate a minimum H₂O content considering the contribution of fluids from the top-most portion of the subducting Cocos plate (the volcanic component and thin sedimentary cover), consistent with the expected fluid-rich environment at the plate interface and the presence of free water (e.g., Bebout & Penniston-Dorland, 2016; Condit et al., 2020; Hernández-Uribe & Palin, 2019).

4.2. Bulk Compositions

4.2.1. Silica Metasomatism of Hydrated Peridotite

We vary the silica content of the serpentinite bulk compositions to simulate the enrichment of these rocks in silica via metasomatism. Across a bulk composition based on an average serpentinized harzburgite from the mantle wedge (Deschamps et al., 2013), we only vary the normalized silica content from that equivalent to hydrated

LINDOUIST ET AL. 6 of 23

/agupubs.onlinelibrary.wiley.com/doi/10.1029/2023GC010981, Wiley Online Library on [09/08/2023]. See the Terms and Conditions (https://onlinelibrary.wiley

Table 1Bulk Rock Compositions in Oxide wt. %

0.11	Serpentinized	Serpentinized	Cocos	Cocos
Oxide	harzburgite C ₀	harzburgite C ₁	sediment	basalt
Na_2O	-	-	2.5	2.05
MgO	39.84	33.34	2.87	8.53
Al_2O_3	0.54	0.45	13.13	16.58
${ m SiO}_2$	39.5	49.37	54.24	49.18
K_2O	-	-	1.23	0.14
CaO	0.29	0.24	1.73	13.34
${ m TiO_2}$	-	-	0.57	0.85
MnO	-	_	2.33	-
FeO	6.83	5.72	8.5	7.26
Fe_2O_3	-	-	2.82	1.54
H ₂ O	13	10.88	_	_

peridotite (39 wt. % SiO_2) to that of MORB (49 wt. % SiO_2). We use the serpentinized harzburgite composition to represent a refractory peridotite composition from the mantle wedge that has been hydrated by slab-derived aqueous fluids. Because the oxidation state of the forearc mantle wedge is poorly constrained, we run the serpentinite model with oxygen fugacity defined by variously reduced and oxidized redox buffers, ranging from $\Delta log_{10}fO_2$ (FMQ) values of -2 to +2 to encompass a range of reported oxygen fugacity estimates for mantle wedge serpentinites (Deschamps et al., 2013). Complete initial (C_0 —hydrated harzburgite) and final (C_1 —silica-metasomatized harzburgite with 49 wt. % SiO_2) bulk rock compositions for both models of silica metasomatism are reported in Table 1.

4.2.2. Silica and Fluid Production From the Cocos Plate

We also model fluid production from subducted lithologies to examine the sources of fluids and silica. Bulk compositions for sedimentary and basaltic rocks are based on samples recovered from boreholes in the modern Cocos plate. Approximately 150 m of sediment and 7 m of basalt were recovered from Hole 487 off the coast of Acapulco during Leg 66 of the Deep Sea Drilling Project (Watkins et al., 1982). The sedimentary rock bulk composition

used here (Table 1) is based on the average bulk composition of the sediment column from Hole 487 reported in Plank and Langmuir (1998), with Fe_2O_3 content estimated from reported total Fe using the average Fe^{3+}/Fe_{Total} ratio of 0.23 for metapelites reported in Forshaw and Pattison (2021). The sedimentary rocks recovered from Hole 487 were hemipelagic—pelagic muds and clays with very little carbonate content (Watkins et al., 1982). The basaltic bulk composition used here (Table 1) is based on an average of three bulk compositions reported for the basalt from Hole 487 (Joron et al., 1982), with Fe_2O_3 content estimated from reported total Fe using the average Fe^{3+}/Fe_{Total} ratio of 0.16 for global average MORB (Cottrell & Kelley, 2011). This MORB composition is comparable to global average MORB compositions (cf. Gale et al., 2013).

4.3. Results of Silica Metasomatism Modeling

Figure 2 shows the results of T-X modeling of silica metasomatism of serpentinized harzburgites at end-member redox conditions. The major minerals (antigorite, olivine, talc) behave comparably in both the reduced (Figure 2a) and oxidized (Figure 2b) models. Antigorite is stable and abundant over almost all of the model space, but antigorite volume begins to decrease with increasing temperature starting around 500°C, with a concomitant increase in olivine abundance until antigorite completely breaks down around 650°C. Petrologic models were also constructed for intermediate redox conditions, but these do not show significant variations from the end-member models. Modeling results of other redox conditions can be found in Figure S1 in Supporting Information S1.

In both oxidized and reduced settings, the addition of silica is required for talc growth in serpentinized harzburgites at the lower temperature conditions of the flat slab beneath Guerrero (Figure 2). From the starting point of \sim 39 wt. %, the silica content must increase to \sim 43 wt. % in both oxidized and reduced settings in order for talc to stabilize. Adding additional silica to the system at these lower temperatures—350–500°C in the reduced model and 350–600°C in the oxidized models—increases the modal abundance of talc in the rock. Plots of the modal abundance of each mineral across the TX model at 450°C for each model indicate that the dominant talc-forming reaction is antigorite + SiO₂ = talc + H₂O (Figures 2e and 2f). From low to high values of silica wt. %, the predicted modal abundance of antigorite decreases at the expense of talc formation (Figures 2e and 2f). To achieve a rheologically significant \sim 10 vol. % talc in the rock, silica contents must be greater than 44–45 wt. % (Figures 2c–2f). At higher temperatures of 580–620°C and greater, 15–20 vol. % talc can grow in serpentinized harzburgites with no additional silica, and greater modal abundance is reached with increasing silica metasomatism compared to lower temperatures.

The stability of minor phases besides antigorite and talc differs between the reduced and oxidized serpentinite models. Minor phases are typically present at less than 5 vol. % (Figures 2e–2f), such as amphibole (dominantly actinolite) and clinopyroxene (dominantly diopside). In the reduced model (Figure 2a), the increased stability of amphiboles between 515 and 585°C results in a relative lower abundance of talc. In particular, between silica

LINDQUIST ET AL. 7 of 23

15252027, 2023, 8, Downloaded from https://agupubs.onlinelibrary.wiley.com/doi/10.1029/2023GC010981, Wiley Online Library on [09/08/2023]. See the Terms and Conditions (https://onlinelibrary.wiley.com/terms-and-conditions) on Wiley Online I

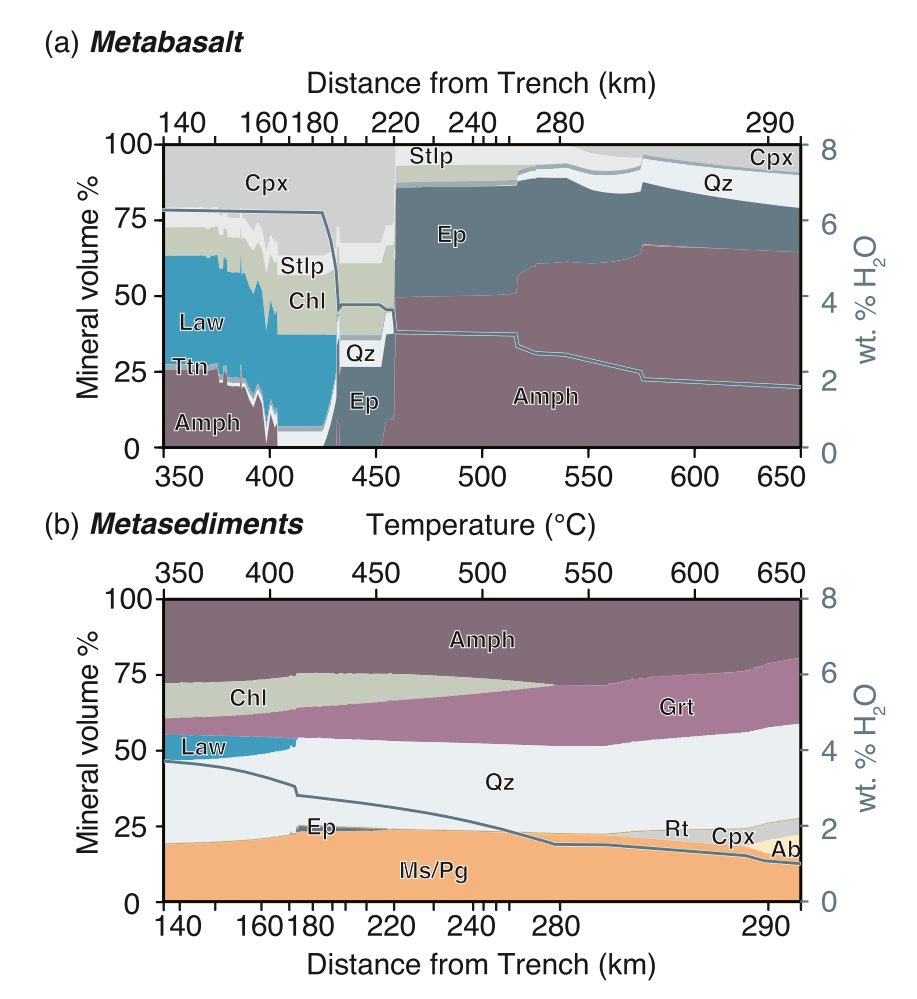


Figure 3. Plots of mineral modal abundance and the weight percentage of mineral-bound water (blue lines) for (a) metabasaltic and (b) metasedimentary rocks from the modern Cocos plate at 1.3 GPa and over the range of temperatures along the flat slab top beneath Guerrero.

contents of 43 and 46 wt. %, talc disappears completely from the system. In the rest of the modeled space, a clinoamphibole phase is predicted to be stable with <3 vol. %, but in this temperature range at $SiO_2 > 43$ wt. %, amphiboles are predicted to constitute up to ~25 vol. % of the rock near 585°C. In the oxidized model (Figure 2b), a single amphibole phase is only ever present at ≤ 3 vol. % over the model space. Although more talc is produced for a given silica content at lower temperatures in the more oxidized model, at high temperatures talc is more abundant in the reduced model for low silica content (Figure 2). At 600°C and 43 wt. % SiO_2 , for example, the reduced model stabilizes 15 vol. % talc, compared to only ~7 vol. % talc in the oxidized model (e.g., Figure 2c vs. Figure 2d).

4.4. Results of Modeling Subducted Lithologies

We also calculated thermodynamic models of metasedimentary and metabasaltic rocks from the subducting Cocos plate using a pressure-temperature path at 1.3 GPa over the range of flat slab temperatures to eventually estimate the volumes of metamorphic fluid production. Figure 3 shows the predicted modal abundance of mineral phases in the basaltic and metasedimentary rocks along this P-T path and the associated amount of mineral-bound water hosted in those phases. Decreases in the wt. % mineral-bound H_2O with increasing temperature in both models is inferred to correspond to fluid release from the subducting Cocos plate. Water-saturated metasedimentary rocks start with less than 4 wt. % H_2O and are predicted to dehydrate continuously along the flat slab segment (Figure 3b), containing \sim 1 wt. % H_2O at 290 km from the trench. In contrast, the metabasalt model starts with 6 wt. % H_2O and exhibit three pulses of dehydration (Figure 3a): (a) at \sim 425°C and 190–200 km from the trench,

LINDQUIST ET AL. 8 of 23

.5252027, 2023, 8, Downloaded from https://agupubs.onlinelibrary.wiley.com/doi/10.1029/2023GC010981,

are governed by the applicable Creative Commons

the breakdown of lawsonite releases >2 wt $\%H_2O$, (b) at \sim 460°C and 220 km from the trench, and (c) 520°C and 270 km from the trench of chlorite breakdown produce >0.5 wt $\%H_2O$ (Figure 3a) at each location. These dehydration reactions occur across very narrow temperature ranges and therefore short distances along the flat slab.

5. Water and Silica Flux and Time-Dependent Talc Production

Using the predicted changes in the quantity of mineral-bound water and assumptions about the geometry and composition of the subducting Cocos plate, we estimate the volume of water released over the flat slab segment beneath Guerrero and the amount of silica that could be advected in solution into the overlying mantle wedge. We also compare this to the silica and water flux required to produce serpentinites with a rheologically significant 10 vol. % talc based on our *T*-X models of metasomatism.

We construct a water and silica flux model based on modern plate velocities and thickness estimates of the rocks that comprise the Cocos plate and the overlying mantle wedge (Section 2.1). Using the thermal model of Manea and Manea (2011), we extract the temperature conditions of the flat plate interface at 40 km depth between 120 and 290 km from the trench. We binned the flat plate interface into 5 km segments, and using the temperature data from the thermal model, we calculate the corresponding water content and rock density from the MORB and metasedimentary Perple_X models. For each segment, the amount of water lost by subducting rocks is calculated as the difference between the maximum and minimum water content (in kg/m³) of the modeled lithology over the temperature range of that 5 km segment. Using the modern convergence rate of 60 km Myr⁻¹ and the thickness of the water-producing rock (150 m of metasediments, 600 m extrusive basalt), we calculate the flux of water across the plate interface in kg m⁻² Myr⁻¹. This model assumes that all fluid released during metamorphism in a given 5 km-long region of the subducting Cocos plate is transported vertically into the overlying 5 km-long region of the subduction interface.

The structure of the subducting Cocos crust—i.e., the thicknesses of the layers of basalt and sedimentary rocks—is assumed to be comparable to what is presently outboard of the trench. We assume that the thickness of the sedimentary rock is 150 m—approximately the thickness of the sediment in hole 487 from the Cocos plate off the coast of Acapulco (Watkins et al., 1982). We use a thickness of hydrated MORB of 600 m, which is assumed to be a representative thickness of the layer of extrusive material based on seafloor drilling (e.g., Jarrard, 2003).

5.1. Water Fluxes

Our water flux estimates show constant low levels of fluid release by the downgoing slab across the plate interface, interspersed with large pulses of water release that are localized where the subducting basalt undergoes metamorphic dehydration. Figure 4a shows the calculated flux of water across the plate interface averaged for each 5 km-long segment of the flat slab, and the relative contributions of metabasalts and metasedimentary rocks. Total water fluxes range from 10^3 to 3.5×10^5 and average 3.9×10^4 kg m⁻² Myr⁻¹ over the whole flat slab. Metabasalts contribute an average of 7.7 times higher flux than metasediments, or 89% of the total water flux over the flat slab, as a result of both the greater volume of metabasalt than metasediments in our model crustal structure and the larger amount of mineral-bound water that can be carried by basaltic lithologies.

As expected from our modeling of subducted Cocos slab lithologies and their water content (Figure 3), water is released from the Cocos plate in three main pulses, one at 180–200 km from the trench, one at 215 km from the trench, and another at 270–290 km. These regions of high fluid flux are associated with the three main pulses of metabasalt dehydration shown in Figure 3. The first pulse of dehydration results in the greatest water fluxes up to 3.5×10^5 , the second pulse up to 1.6×10^5 , and the final pulse up to 1.5×10^5 kg m⁻² Myr⁻¹. In all cases, our models suggest the fluid released from metabasalts is the dominant contributor to the pulse, demonstrating that the dehydration of metabasalts provides a much more significant flux of water into the mantle wedge and along the plate interface than that of metasedimentary rocks, as has been observed in previous modeling studies (e.g., Condit et al., 2020).

5.2. Silica Fluxes

We combine the estimates of the water flux into the mantle wedge over the flat slab segments with an empirical model of silica solubility in water (Manning, 1994) to calculate the amount of silica that could be advected

LINDQUIST ET AL. 9 of 23

15252027, 2023, 8, Downloaded from https://agupubs. onlinelibrary.wiley.com/doi/10.1029/2023GC01981, Wiley Online Library on [09/08/2023]. See the Terms and Conditions (https://onlinelibrary.wiley.com/terms-and-conditions) on Wiley Online Library for rules of use; OA articles

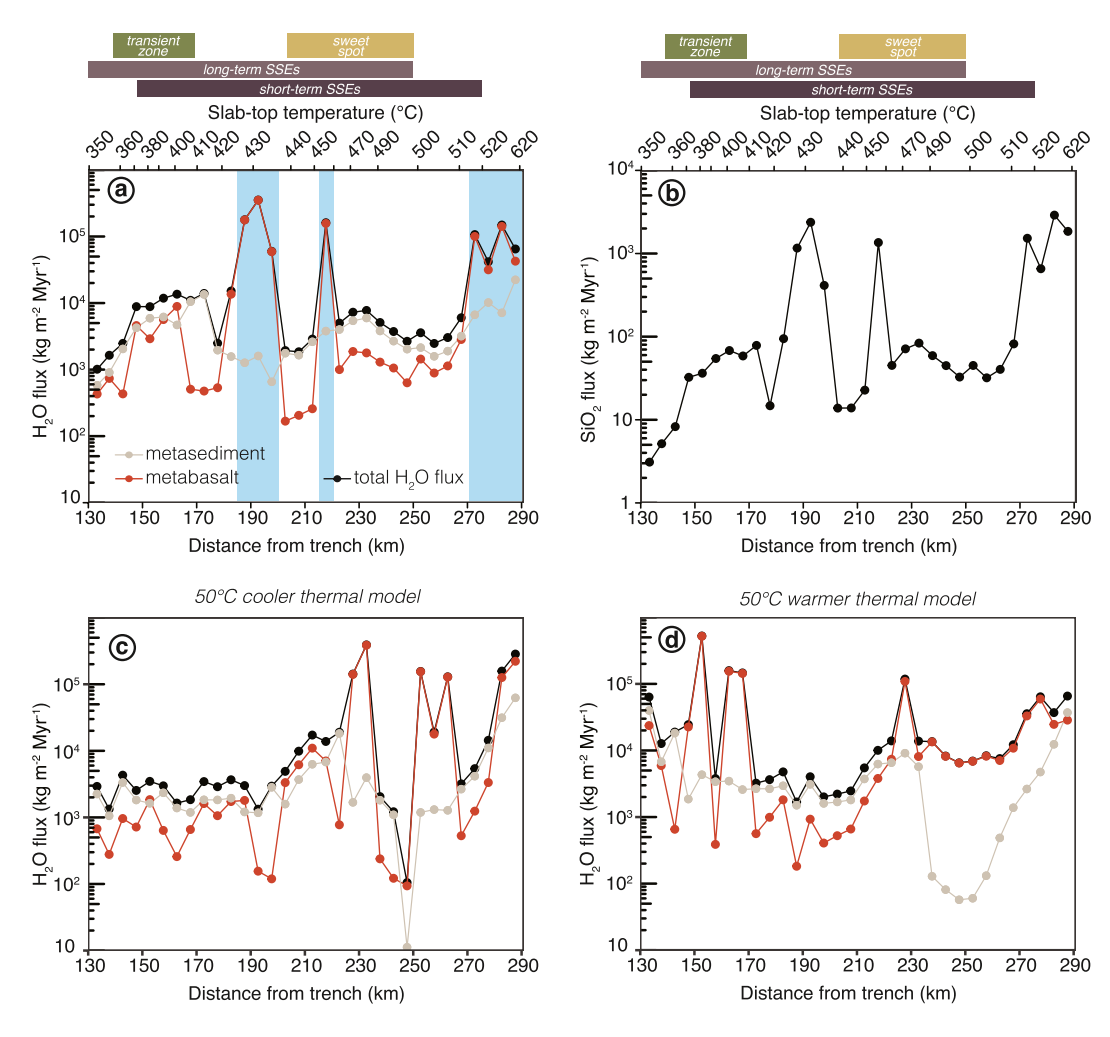


Figure 4. Estimates of (a) water and (b) silica flux across the plate interface assuming vertical transport of all fluids released by the slab into the overlying interface. (a) Shows the relative contributions to water flux of metasedimentary and metabasaltic rocks in the Cocos plate. Regions highlighted in blue are the main areas of high water flux into the plate interface. (c, d) Show the effects of 50°C cooler and warmer thermal models, respectively, on the locations of water flux pulses, shifting the locations of large water and silica flux into the interface by up to 50 km from the original model in panel (a).

from the subducting Cocos plate into the plate interface serpentinites. Assuming that all the silica that could be advected is added to the serpentinized harzburgites in the plate interface—which is reasonable given the silica undersaturation of peridotites—we calculate a silica mass flux across each 5 km segment of the flat plate interface (Figure 4b). These calculations assume silica saturation of a pure $\rm H_2O$ fluid that is transported vertically into the plate interface.

Our model only considers the advection of silica in aqueous fluids, so the pattern of silica flux (Figure 4b) generally follows the pattern of water flux (Figure 4a), with low levels of silica flux along the entire flat slab punctuated by pulses of high silica flux where dehydration occurs in the subducting metabasalts. This silica flux is also dependent on temperature, which has a strong influence on the solubility of silica in aqueous fluids (e.g., Manning, 1994). In both models, only eight of the 5-km wide bins exhibit higher than average silica fluxes. As with the water flux, there are three primary regions of silica flux around 180-200, 215, and 270-290 km from the trench, and because silica solubility increases with temperature, silica flux is greater farther from the trench as the slab top continues to heat up. Silica flux across the plate interface ranges from 3.1 to 2,900 and averages $410 \text{ kg m}^{-2} \text{ Myr}^{-1}$ across the entire flat slab. The first high-flux pulse of fluids around 190 km from the trench results in silica fluxes up to $2,400 \text{ kg m}^{-2} \text{ Myr}^{-1}$. The second pulse at 215 km reaches $1,400 \text{ kg m}^{-2} \text{ Myr}^{-1}$, and the final pulse from 270 to 290 km contributes up to $2,900 \text{ kg m}^{-2} \text{ Myr}^{-1}$ (Figure 4b).

LINDQUIST ET AL. 10 of 23

onlinelibrary.wiley.com/doi/10.1029/2023GC010981,

Wiley Online Library on [09/08/2023]. See the Terms

Additionally, recognizing that thermal models at these depths are associated with uncertainties of $\pm 50^{\circ}$ C (Peacock, 2009), we also calculate water flux from the subducting slab in a 50°C cooler (Figure 4c) and 50°C warmer (Figure 4d) thermal structure. These models provide an indication of the sensitivity of the predicted locations of dehydration pulses to the thermal structure of the subduction zone and uncertainties in thermodynamic modeling approach and the compositional variability of subducting rocks. As Figures 4c and 4d show, a hotter or colder thermal model for Guerrero may shift the locus of dehydration—and therefore fluid and silica flux—by tens of kilometers in some cases. We further consider the implications of this uncertainty and sensitivity in the discussion.

5.3. Time Dependent Talc Production by Pervasive Fluid Flow

The estimated silica fluxes from the subducting slab then allow us to build a simple time-dependent model for talc production at the plate interface. We use this to predict the growth of talc along the flat slab over its minimum lifetime of 10 Myr (Ferrari et al., 2012). Pairing the silica flux estimates with our models of silica metasomatism, we can estimate the silica content of the serpentinite along the plate interface in million-year increments and determine the modal abundance of talc for the corresponding *T-X* conditions. When considering the effects of these fluids on the bulk rock composition of serpentinites, we use two end-member models for the thickness of the overlying mantle material: a 4 km-thick zone of serpentinite based on the thickness of the observed low-velocity layer (Kim et al., 2010; Song et al., 2009); and a 100 m-thick zone. We use this range of thicknesses to simulate silica-bearing fluids reacting with different volumes of hydrated peridotite. This allows us to explore the effect of different interactive volumes at the plate interface on the ability of the zone to grow significant quantities of rheologically important minerals. The thinner 100 m-thick zone endmember may be a more geologically realistic interaction volume and reflect the possible confinement and channelization of fluids at the plate interface (e.g., Bebout, 1991; Ganzhorn et al., 2019). However, to compare with the geophysical interpretations of Kim et al. (2010), we include the 4 km-thick model endmember as well.

Figure 5 displays the results of this time-dependent metasomatism model for each endmember oxygen fugacity and interface thickness parameter by plotting the initial wt. % SiO₂ in serpentinites for each 5 km segment of the flat slab and the final SiO₂ content after 10 million years, as well as the corresponding talc abundance. For reference, we also extract from each T-X model of silica metasomatism the values of SiO₂ content at which the serpentinite achieves 10 vol. % talc at the conditions of each 5 km segment (Figure 5). As with the silica flux models, these calculations are based on the assumption that silica is advected in a pure H_2O fluid that is transported vertically into the plate interface. We further assume that the silica is homogeneously mixed with the serpentinite at the interface, where it instantaneously reacts to increase the silica content of the serpentinite. Therefore, these models only inform us of the potential for talc production by advective silica metasomatism through pervasive fluid flow.

For both reduced and oxidized serpentinites at the plate interface, the flux of silica into the 4 km-thick interface is not high enough anywhere along the flat slab to produce any appreciable talc in the plate interface after 10 million years. Assuming pervasive metasomatism of the 4 km-thick interface, the added silica would be too dilute to drive the bulk composition of the serpentinite to greater wt. % SiO₂ (Figures 5a and 5b). In the 100 m-thick interface model, however, the magnitude of silica flux relative to the volume of interface rock is high enough to drive up the silica content of the serpentinite (Figures 5c and 5d). In this case, talc is produced in the serpentinite at the interface in the regions that experience large fluid fluxes at 180–200, 215, and 270–290 km from the trench.

Larger volumes of talc are stabilized by the oxidized serpentinites than the reduced serpentinites. In the first fluid pulse around 190 km, 27 vol % talc is produced in the reduced serpentinite compared to 33 vol. % talc in the oxidized serpentinite, and similarly at 280 km from the trench, up to 33 vol. % talc is produced compared to up to 43 vol. % talc in the oxidized serpentinite model (Figures 5c and 5d). At the fluid pulse near 215 km from the trench, only the oxidized model achieves 10 vol % talc.

It should be noted that the wt. % SiO₂ values reported in Figure 5 are the amount of silica in the model rock, which is different from the wt. % SiO₂ values reported in Figure 2 that are the total amount of silica in our modeled system. The difference between these is a function of the amount of mineral-bound water, as the total amount of water in the system is fixed. Temperature-dependent differences in the amount of water that is mineral-bound in serpentinite accounts for the variations in the starting SiO₂ content of serpentinites in both reduced and oxidized models of metasomatism (Figure 5).

LINDOUIST ET AL. 11 of 23

15252027, 2023, 8, Downloaded from https://agupubs.onlinelibrary.wiley.com/doi/10.1029/2023GC010981, Wiley Online Library on [09/08/2023]. See the Terms and Conditions (https://onlinelibrary.wiley.com/term

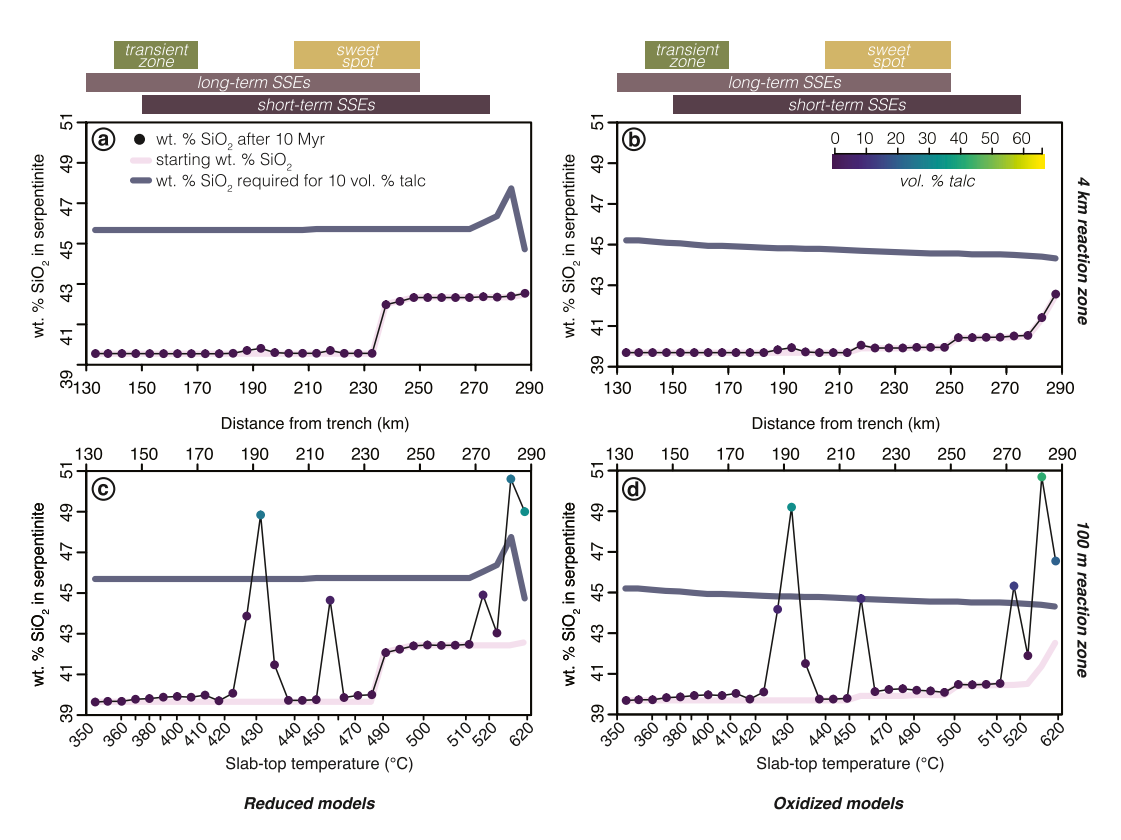


Figure 5. Models of the amount of talc in serpentinites at the plate interface based on flux estimates into 4 km (top panels) and 100 m thick (bottom panels) plate interface zones from Figure 4, and reduced and oxidized serpentinite metasomatism models in Figure 2, assuming 10 Ma of flat slab subduction and adjective silica flux into the plate interface. Light pink lines show the amount of silica that serpentinites at the plate interface start with before the addition of silica-rich fluids, circles show the amount of silica predicted after 10 Ma of subduction and fluid flow and are colored according to the modal abundance of talc on the same scale from Figure 2, and dark blue lines show the threshold of silica required to produce a rheologically significant 10 vol. % talc for that part of the flat slab.

Our simple time-dependent models show that talc production over 10 million years of flat slab subduction beneath Guerrero is limited by generally low silica fluxes due to low water production and silica solubility systematics along the length of the flat slab segment. Appreciable talc growth through 10 million years of pervasive silica metasomatism is only predicted to occur if the interface is thin so that there is a low interaction volume for the advected silica to metasomatize. Even so, areas of the interface that can achieve ≥ 10 vol. % talc in 10 Myr are localized to regions where the subducting Cocos plate undergoes large pulses of dehydration that can produce sufficient volumes of silica-rich fluids (Figures 5c and 5d).

5.3.1. Calculating Fluxes Required for Significant Talc Volume

Given the values of silica content at which our modeled serpentinites achieve 10 vol. % talc, we also perform a back-calculation to estimate the silica and water fluxes required at each 5 km segment of the flat slab to achieve this rheologically significant abundance of talc within 10 million years. We take the difference between the silica content of the serpentinites with 10 vol. % talc and their initial, unaltered silica contents to determine the silica flux necessary to produce $\geq 10\%$ vol. talc in 10 million years for both reduced and oxidized models (Figure 6a). Again using the silica solubility model of Manning (1994), we calculate the amount of water necessary to advect this target quantity of silica every million years (Figure 6b). Figure 6 compares both target and predicted silica and water fluxes for the flat plate interface.

As expected, over the whole flat slab, the fluxes predicted by our mass balance calculations are much lower than these target silica and water fluxes for a 4 km-thick serpentinite interface. For example, even with the high silica fluxes at 190 km from the trench, the needed silica fluxes to the 4 km-thick interface are \sim 27 times larger than those predicted (Figure 6a). These silica fluxes would then require corresponding water fluxes into a 4 km-thick interface on the order of 10^6-10^7 kg m⁻² Myr⁻¹ (Figure 6b), which are \sim 10–10⁴ times greater than

LINDOUIST ET AL. 12 of 23

15252027, 2023, 8, Downloaded from https://agupubs.onlinelibrary.wiley.com/doi/10.1029/2023GC010981, Wiley Online Library on [09/08/2023]. See the Terms and Conditions (https://onlinelibrary.wiley.com/term

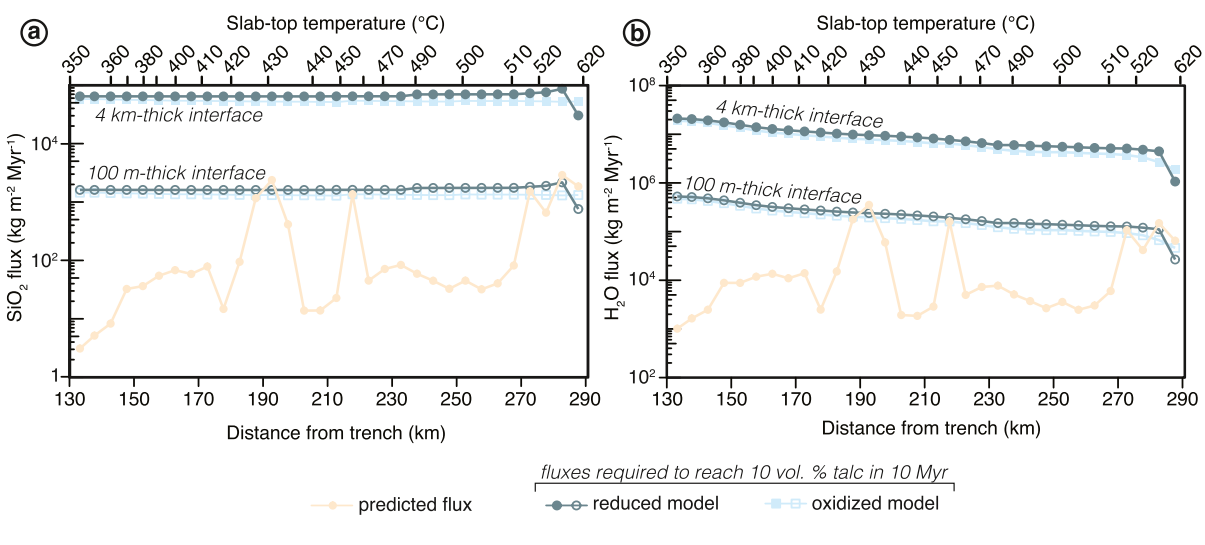


Figure 6. Estimates of the necessary (a) silica and (b) water fluxes into the plate interface to stabilize 10 vol. % talc in serpentinites along the flat slab beneath Mexico in 10 million years. Dark blue circles and light blue squares plot the necessary fluxes for reduced and oxidized models, respectively, and closed and open shapes correspond to the target fluxes for a 4 km-thick and 100 m-thick interface, respectively.

the water fluxes actually predicted (Figure 4a). In contrast, silica fluxes needed to produce significant talc in a 100 m-thick interface average around 1,600 kg m⁻² Myr⁻² (Figure 6a), which corresponds to target water fluxes of $\sim 10^3 - 10^4$ kg m⁻² Myr⁻². As demonstrated in the previous section, our predicted fluxes into a 100 m-thick interface match or exceed these values in three locations (Figure 6), corresponding again to the locations of dehydration pulses in subducting metabasalt.

5.4. Time-Dependent Talc Production by Localized Metasomatism at the Plate Interface

Whereas the previous section considered the effects of metasomatism by pervasive fluid flow resulting in the homogeneous distribution of silica through a prescribed thickness of serpentinite, we may also consider the case of localized metasomatism at the plate interface. In this case, all silica in the fluid released by the Cocos plate reacts with the serpentinite immediately at the plate interface and is scrubbed from the infiltrating fluid to produce a nearly pure talc schist with a bulk composition with ~61 wt. % SiO₂. Using the predicted

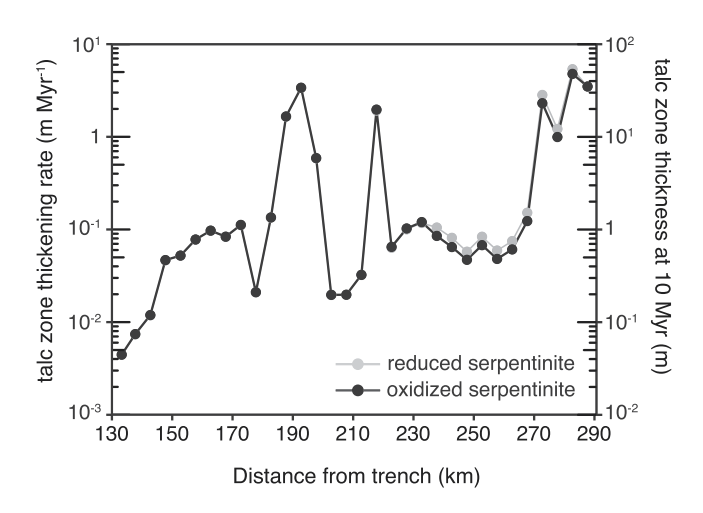


Figure 7. Calculated rate at which a zone of talc schist (96–98 vol % talc) at the plate interface would thicken for reduced (gray) and oxidized (black) serpentinites based on the predicted silica fluxes in Figure 4b. Full thicknesses of the zones of talc schist after 10 Myr are given by the scale on the right.

silica flux from the Cocos plate, we estimate what the thickness of a talcrich layer of rock at the plate interface would be as a result of this type of metasomatism.

Again using serpentinite T-X models, we calculate the difference between the silica content (kg m⁻³) of an ultra-silicified serpentinite with the maximum amount of talc it could have (96-98 vol. % talc at ~61 wt. % SiO₂) and the initial silica content of serpentinites along the flat slab beneath Mexico (Figure S2 in Supporting Information S1). Dividing the predicted silica flux from the Cocos plate by this difference in silica content yields a value for the rate at which a zone of talc schist would vertically thicken at the plate interface (Figure 7). These results indicate talc zone growth rates ranging from 4.4×10^{-3} m Myr⁻¹ where silica fluxes are low closer to the trench, up to 5.4 m Myr⁻¹ where dehydration reactions produce large pulses of silica-rich fluid. Because we calculate this vertical growth rate of a layer of nearly pure talc, this represents a minimum growth rate for a talc-rich layer at the plate interface, as layers containing less talc would require less silica, allowing for thicker talc-rich zones. Over 10 Myr, this would result in the growth of ~50 m-thick layers of talc schist at the high-flux regions of the plate interface, or on the order of several meters on average over the entire flat slab top.

LINDQUIST ET AL. 13 of 23

15252027, 2023, 8, Downloaded from https://agupubs

Wiley Online Library on [09/08/2023]. See the Terms

6. Discussion

6.1. Silica Metasomatism of Serpentinites

Based on geophysical observations of the subduction zone beneath Guerrero, Mexico, a layer of talc has been inferred at the flat plate interface that hosts slow slip and tremor events (Kim et al., 2010). Our T-X models of serpentinized harzburgites at the conditions of the flat slab top beneath Mexico indicate the necessary extent of advective silica metasomatism to producing significant quantities of talc at this plate interface through advective silica metasomatism (Figure 2). For any talc to be present on the flat plate interface where slow slip and tremor occur beneath Guerrero—up to 520°C at 1.3 GPa—our calculations indicate that the silica content of hydrated serpentinites must increase from ~39 to ~43 wt. %. The initial production of talc in these rocks is associated with the breakdown of clinopyroxene in the reduced model and the breakdown of antigorite in the oxidized model. Subsequent increases in talc in both sets of calculations are associated with decreasing abundance of antigorite. To stabilize 10 vol. % talc at the plate interface, serpentinites must achieve ~45 wt. % SiO₂. This amount of talc would be rheologically significant and would likely localize deformation at the plate interface (e.g., Hirauchi et al., 2013; Peacock & Wang, 2021). Over the temperature range of slow slip and tremor phenomena on the flat slab (~350-520°C), each additional 1 wt. % SiO₂ in the serpentinized harzburgites will stabilize an additional 5 vol. % talc, and increasing the silica content of these to that of MORB (~49 wt. % SiO₂) stabilizes up to 35-40 vol. % talc (Figures 2c and 2d). Chlorite, another weak phyllosilicate mineral that may influence the rheology of the plate interface, is not predicted to stabilize in our serpentinite models until >625°C, which is only reached at the farthest end of the flat slab from the trench.

Our results give us a lower bound for the amount of silica metasomatism needed to produce rheologically significant talc within hydrated entrained mantle wedge peridotites along the flat slab. These results are not significantly affected by redox state: our two end-member models for the redox state of serpentinite at the flat plate interface both show that the stability of talc in *T-X* space and the amount of silica necessary to produce talc only vary slightly between these two models (Figure 2). In evaluating the ability of silica-rich water produced by the predicted dehydration reactions in our models in the next section, we keep both oxidation state end-member models in mind to understand the range of conditions that may allow the stabilization of large volumes of talc near the plate interface through silica-metasomatism.

6.2. Water and Silica Flux at Guerrero

6.2.1. Fluid Production and Slip Behaviors

The production of metamorphic fluid through dehydration reactions is influenced by both the bulk rock compositions from the subducting slab in Guerrero and the P-T path these rocks take as they subduct. Both metasedimentary and metabasaltic rocks of the Cocos plate near the flat plate interface will undergo dehydration reactions and produce water in three pulses along the flat slab (Figures 3 and 4). The first pulse of fluid flux into the interface is the result of lawsonite and clinopyroxene breakdown into epidote and chlorite at \sim 425°C. The second pulse is associated with chlorite breakdown at \sim 460°C, and the third with chlorite, epidote, \pm stilpnomelane breakdown over 520–575°C. Although this last pulse occurs over a wider temperature range, these temperatures occur at the end of the flat slab region near the mantle wedge where the flat slab top heats up rapidly through these temperatures so that they occur within a 20 km region along the slab top. The minerals that are predicted to carry water in both the sedimentary and basaltic rocks of the Cocos plate are consistent with those in other petrologic studies of slab dehydration (e.g., Condit et al., 2020; Hernández-Uribe & Palin, 2019; Kerrick & Connolly, 2001).

The locations of the two pulses of fluid production nearest the trench lie within the spatial extent of both long-term and short-term SSEs. These fluids will carry silica that will likely metasomatize rocks at the plate interface, as discussed in the next section, and will contribute to the elevation of pore fluid pressures at the plate interface. Two of the main fluid pulses, at 180–200, and 270–290 km from the trench, are anti-correlated with the location of the primary regions of tremor activity: the transient zone and sweet spot 140–170 and 205–250 km from the trench, respectively (Figure 4). However, the middle pulse that our models predict at 215 km from the trench lies in the range of the tremor sweet spot. Both short- and long-term SSEs overlap the predicted locations of the two main fluid pulses nearer the trench from our models (Figure 4). However, both types of SSEs occur over much wider regions than the extent of the water and silica pulses. While considering uncertainties in thermal structure that may shift the location of these pulses within the zones of SSEs (Figures 4c and 4d), the spatial extents of local water and silica flux pulses into the plate interface are much narrower than those of SSEs.

LINDOUIST ET AL. 14 of 23

.com/doi/10.1029/2023GC010981,

Our results also show that the water production by metasedimentary rocks is significantly lower than that of metabasaltic rocks. In particular, each of the major pulses of water is dominated by fluids produced from the dehydration of metabasalts (Figures 4a and 4b). This is consistent with the results of other authors (Manea & Manea, 2011; Perry et al., 2016), although the degree of dehydration for the modeled metabasalts considered here is greater because of the geologically realistic assumption of water-saturated conditions near the plate interface. Although this means that our calculations consider the maximum amount of water that could be carried by sedimentary and basaltic rocks in the Cocos plate, we only consider the contribution of water from the upper 600 m of volcanic rocks that make up the oceanic crust. Deeper portions of the oceanic crust are likely hydrated heterogeneously along fault zones that may penetrate into the mantle lithosphere as observed at other subduction zones (e.g., Naif et al., 2015). The release of these fluids from the oceanic lower crust and suboceanic mantle may also contribute to the water flux into the plate interface (e.g., Gutiérrez-Aguilar et al., 2022).

6.2.2. Silica Flux and Magnitude of Talc Metasomatism

Given the predicted fluid and silica flux from the Cocos plate, our models of time-dependent silica enrichment of serpentinites beneath Guerrero for end-member interface thicknesses of 100 m to 4 km (Sections 5.3 and 5.4) predict the locations and potential magnitudes of talc production along the flat plate interface. With the silica fluxes that we calculated from the dehydration potential of the subducting slab, we find that our simple advective model of silica metasomatism does not predict pervasive talc production along the entire flat slab interface, which should be analogous to the low velocity layer of Kim et al. (2010).

The extent of silica enrichment depends both on the thickness of the serpentinite layer (i.e., the volume of rock with which fluids interact) and the oxidation state of these serpentinites (Figure 5). The results of our time-dependent models show that after 10 million years of flat-slab subduction, talc production by this pervasive fluid flow can only occur in thin (\sim 100 m) interface zones and is localized to portions of the flat slab where dehydration reactions in the subducting slab liberate large volumes of water. At these regions of major fluid production, serpentinized harzburgites in a 100 m-thick zone may experience increases in silica content from 39 to \sim 50 wt. % SiO₂ after 10 million years of fluid and silica flux from the subducting Cocos plate (Figure 5). Oxidation state then influences the amount of talc that may be produced by similar changes in the silica content of reduced and oxidized serpentinites, with the latter generally stabilizing greater volumes of talc.

Importantly, it is difficult to produce rheologically significant quantities of talc in the 4km thick interface models or enough talc to explain the seismic observations. In neither reduced nor oxidized models of pervasive silica metasomatism of a 4 km-thick zone does significant talc stabilize because the amount of silica introduced into the interface is not high enough to drive the silicification of such a large volume of serpentinite (Figure 6). These results suggest that, by itself, talc production by advection of silica from the subducting slab into the plate interface cannot explain the low Vp/Vs ratios and low Vs values in the ~4 km-thick layer imaged by Kim et al. (2010).

Considering our model of localized silica metasomatism at the plate interface (Section 5.4), however, it is possible that meter-scale layers of talc-schist can grow immediately at the plate interface as silica-rich fluids react with "fresh" serpentinites and are scrubbed of silica (Figure 7a). Unlike the other models based on pervasive fluid flow and homogeneous metasomatism of prescribed thicknesses of serpentinite (Figures 5 and 6), localized metasomatism at the plate interface would produce a layer of talc schist along the entire flat plate interface beneath Mexico. With an average thickness after 10 Myr of \sim 7 m (Figure 7b), such a zone of talc-rich rock is consistent with the geologic record of talc schists in exhumed subduction zone rocks, which typically occur in layers tens of centimeters to meters thick (e.g., Hirauchi et al., 2020; Hoover et al., 2022; Spandler et al., 2008).

In addition to the amount of silica introduced to the plate interface, oxidation state of the rocks at the plate interface may influence the effects of metasomatism (and vice versa). Oxidized serpentinites generally can stabilize larger volumes of talc than reduced serpentinites with the same silica content (Figure 2), and in our time-dependent models oxidized serpentinites do indeed achieve more talc than reduced serpentinites (Figure 5). The redox conditions of serpentinites in the mantle wedge are not well constrained (Deschamps et al., 2013), but more serpentinized peridotites are likely to be more oxidized with higher Fe³⁺/Fe_{total} than fresh peridotites (Evans, 2008). Our oxidized *T-X* models may thus more closely represent the mineralogy of serpentinites at the plate interface in the Mexican subduction zone. However, the control of redox conditions on the abundance of talc at the plate interface mainly becomes significant at high temperatures, and the difference between oxidized and reduced models is thus not as relevant to the majority of the area of the flat slab that hosts ETS.

LINDOUIST ET AL. 15 of 23

15252027, 2023, 8, Downloaded from https://agupubs

.wiley.com/doi/10.1029/2023GC010981,

Wiley Online Library on [09/08/2023]. See the Terms

6.2.3. Sensitivity of Fluid Production to Thermal Structure

As Figures 4c and 4d show, our predicted locations of dehydration are extremely sensitive to changes in the thermal model as shown in other subduction-related petrologic models (e.g., Hernández-Uribe & Palin, 2019; Kerrick & Connolly, 2001). In particular, the low thermal gradient down-dip along the top of the flat slab beneath Guerrero may result in large spatial uncertainties in the location of water and silica fluxes. For the water flux pulses centered at 190 and 215 km from the trench, this 50°C uncertainty has the potential to shift these loci of dehydration by ±40–50 km from the trench. The large pulse of fluids and silica that we predict occurs at the northeast end of the flat slab could be shifted 60 km trenchward if temperatures at the flat slab are 50°C higher than predicted in the thermal model that we use. This would place this large fluid pulse in the region of the tremor sweet spot. Therefore, it is difficult to definitively correlate the predicted locations of dehydration pulses with the distribution of slow slip phenomena at the plate interface. Even when considering the uncertainties in the exact location of dehydration reactions in the downgoing Cocos plate, however, the location of the water flux pulse nearest to the trench is always encompassed by the slip areas of both the short- and long-term SSEs (Figure 4).

Previous petrologic modeling has also shown that the dehydration of metabasalts and metasedimentary rocks should provide significant pulses of fluid to the plate interface beneath Guerrero (Condit et al., 2020; Manea & Manea, 2011; Manea et al., 2004; Perry et al., 2016), although the predicted locations of dehydration pulses differ from the results of the models presented here. Manea and Manea (2011) and Perry et al. (2016) construct their own models for the thermal structure of the subduction zone at Guerrero. Perry et al. (2016) consider the added effect of fluid circulation in the subducting oceanic lithosphere in their models, which accounts for at least some of the difference between our predictions of fluid flux from the dehydrating oceanic lithosphere. The preferred model of Perry et al. (2016) predicts pulses of fluid flux near 140, 225–275, and >300 km from the trench. Manea and Manea (2011) predict that the majority of dehydration in the metasedimentary and metabasaltic rocks occurs between 230 and 250 km from the trench. This range overlaps with landward-end of the tremor sweet spot, from 205 to 250 km from the trench (Frank et al., 2014); however, neither of these two studies pairing petrologic and thermal models at Guerrero have considered the effects of uncertainty in the thermal models that clearly can have a large impact on the predicted locations of dehydration reactions (Figures 4e and 4f). In this work, we use the thermal model of Manea and Manea (2011) to establish the P-T parameters of our petrologic modeling; therefore, the differences between our models and those of Manea and Manea (2011) may be due to differences in bulk compositions and phase-equilibrium model parameters. Manea and Manea (2011), for example, use phase diagrams from Rüpke et al. (2004), who used bulk compositions of global average sediment compositions for metasedimentary models, and average carbonate-altered MORB from the Atlantic Ocean for metabasalt models, and constructed these models using an earlier generation thermodynamic database. These differ slightly in bulk composition from the local sedimentary and basaltic rocks of the Cocos plate near Guerrero that we use here, and this compositional variation likely contributes to the differences between our petrologic predictions.

6.3. Assumptions and Caveats

Both our petrologic models and mass balance calculations rely on several assumptions that are important to consider in interpreting these results. The petrologic models that form the foundation of this work assume that rocks are in thermodynamic equilibrium and thus do not account for the potential effects of reaction overstepping. However, as considered by Condit et al. (2020), rocks near the plate interface are likely to experience metamorphic reactions close to equilibrium P-T conditions because of the abundance of fluids, additional strain energy contributed through deformation, and, when considering the devolatilization of the subducting plate, dehydration reactions that are associated with large entropy changes which reduce the magnitude of reaction overstepping. Nonetheless, in phase equilibria modeling, 2σ uncertainties of $\pm 50^{\circ}$ C and ± 0.1 GPa in the location of phase assemblage field boundaries are also expected as a result of uncertainties associated with end-member thermodynamic properties and the development of activity-composition models (e.g., Gervais & Trapy, 2021; Palin et al., 2016; Powell & Holland, 2008).

Our modeling of the silica metasomatism of serpentinites at the plate interface is also necessarily simplified in several respects. In our first set of analyses, we take a bulk-rock approach by assuming that silica enrichment occurs homogeneously throughout a body of rock. This effectively assumes that fluid flow is pervasive and occurs along grain boundaries, but does not account for the possibility of anisotropic fluid movement through highly deformed rocks (e.g., fracture networks, shear zones), which would be especially likely in the case of our

LINDOUIST ET AL. 16 of 23

onlinelibrary.wiley.com/doi/10.1029/2023GC010981,

localized silica metasomatism models producing meter-scale zones of talc schist (e.g., Figure 7). The channelization and transport of fluids over 10s of kilometers along the plate interface has been documented in various exhumed subduction records (e.g., Angiboust et al., 2014; Bebout & Penniston-Dorland, 2016). As demonstrated in our modeling of water and silica flux into the plate interface, if the fluids that we predict to be produced by the subducting plate interact with smaller volumes of serpentinite, it is easier to drastically change the bulk composition of these rocks and produce talc. However, this bulk-rock approach to modeling the mineralogy of the plate interface under Guerrero is consistent with the uncertainties of geophysical observations, which are only able to resolve low-velocity zones with thicknesses on the order of kilometers. Producing a 3–5 km-thick zone of talcrich serpentinite as predicted by Kim et al. (2010) requires extensive alteration that is appropriately modeled by varying the bulk-rock composition of rocks at the plate interface.

The silica metasomatism models also assume that the only chemical change in the rocks is the addition of silica to the composition of the serpentinites and that the fluid is pure H_2O . Talc may also be produced by the reaction of CO_2 with serpentinites (e.g., Okamoto et al., 2021); however, because of the lack of carbonate materials in sediments recovered from the Cocos plate (Watkins et al., 1982), we suggest that this is unlikely to be a significant process beneath Guerrero. Water is also expected to be the most abundant volatile comprising fluids released by the subducting slab, but solutes such as Al and Ca, in addition to Si, will also be present in these fluids (Codillo, Klein, & Marschall, 2022; Manning, 2004). The involvement of these elements could promote the growth of other minerals like chlorite, which was predicted to grow during some types of metasomatism based on reactive transport modeling (Codillo et al., 2022b), and is a common phase in metasomatic rocks exhumed from subduction zones that may be involved in the localization of deformation at the conditions of ETS (e.g., Hoover et al., 2022; Nishiyama et al., 2023; Ujiie et al., 2022). However, rheological modeling (French & Condit, 2019) and geologic evidence (Hoover et al., 2022) suggest that talc schists may preferentially localize deformation at slow slip strain rates over chlorite schists.

The mass-balance-based models of water and silica flux (Figures 4–7) assume that all the fluid being produced in each 5 km segment of the subducting slab is going directly into the corresponding 5-km segment of the overlying mantle. This approach ignores the possibility of fluid transport along the plate interface. Furthermore, because this model is based on the solubility of silica in pure water, and subduction zone fluids likely carry multiple solutes (Manning, 2004), this calculation likely provides a lower bound on the quantity of silica that would realistically be advected in solution by fluids released from the dehydrating slab. Using the modern convergence rate of 60 mm/yr in estimating water and silica flux is also conservative because Cocos–North American plate convergence rates have been faster in the last 20 Ma (Sdrolias & Müller, 2006).

6.4. Implications for Guerrero and Beyond: Talc Metasomatism and Slip Behaviors

The simple model of silica advection beneath Guerrero that we present here suggests that silica-rich fluids produced by local dehydration in the upper <1 km of the subducting Cocos plate can alter the composition of overlying serpentinites enough to produce significant volumes of talc in these rocks. These predicted areas of talc production, however, are localized to the regions where increasing temperature causes the metamorphic dehydration of subducting metabasalts (Figure 8). If talc is necessary to produce the observed low seismic velocity regions at Guerrero, local fluid and silica fluxes alone cannot explain the hypothesized alteration because silica fluxes are not high enough to increase the silica content of serpentinites to ≥43 wt. % along the entire region of the flat slab where the low velocity zone is imaged (Figure 5). This suggests that either other mechanical and chemical processes contribute to the transfer of silica from the subducting Cocos plate into the overlying plate interface, or that the low Vp/Vs ratios and low Vs values imaged at the plate interface beneath Guerrero (Kim et al., 2010) may be produced by some combination of talc, other minerals, fluids, and rock structures. The 4 km-thick zone may also not reflect the size of the actively deforming and metasomatism region, but rather may be the result of progressive underplating of material, including thinner talc-rich zones, through time.

Although our models predict that the local advection of silica-rich fluids from the subducting slab into the plate interface is insufficient to produce thick talc-rich zones along the entire plate interface beneath Guerrero, it is possible that the migration of fluids within the plate interface may help to distribute silica and promote metasomatism in regions that are not directly adjacent to rocks in the subducting plate that undergo large dehydration reactions (Figure 8). This process is consistent with geophysical observations at Guerrero, where variations in the rate of low-frequency earthquakes during SSEs may be explained by the migration of pulses of pore fluids

LINDOUIST ET AL. 17 of 23

15252027, 2023, 8, Downloaded from https://agupubs.onlinelibrary.wiley.com/doi/10.1029/2023GC010981, Wiley Online Library on [09/08/2023]. See the Terms and Conditions (https://onlinelibrary.wiley.com/terms-and-conditions) on Wiley Online Library for rules of use; OA articles are governed by the applicable Creative Commons Licenses

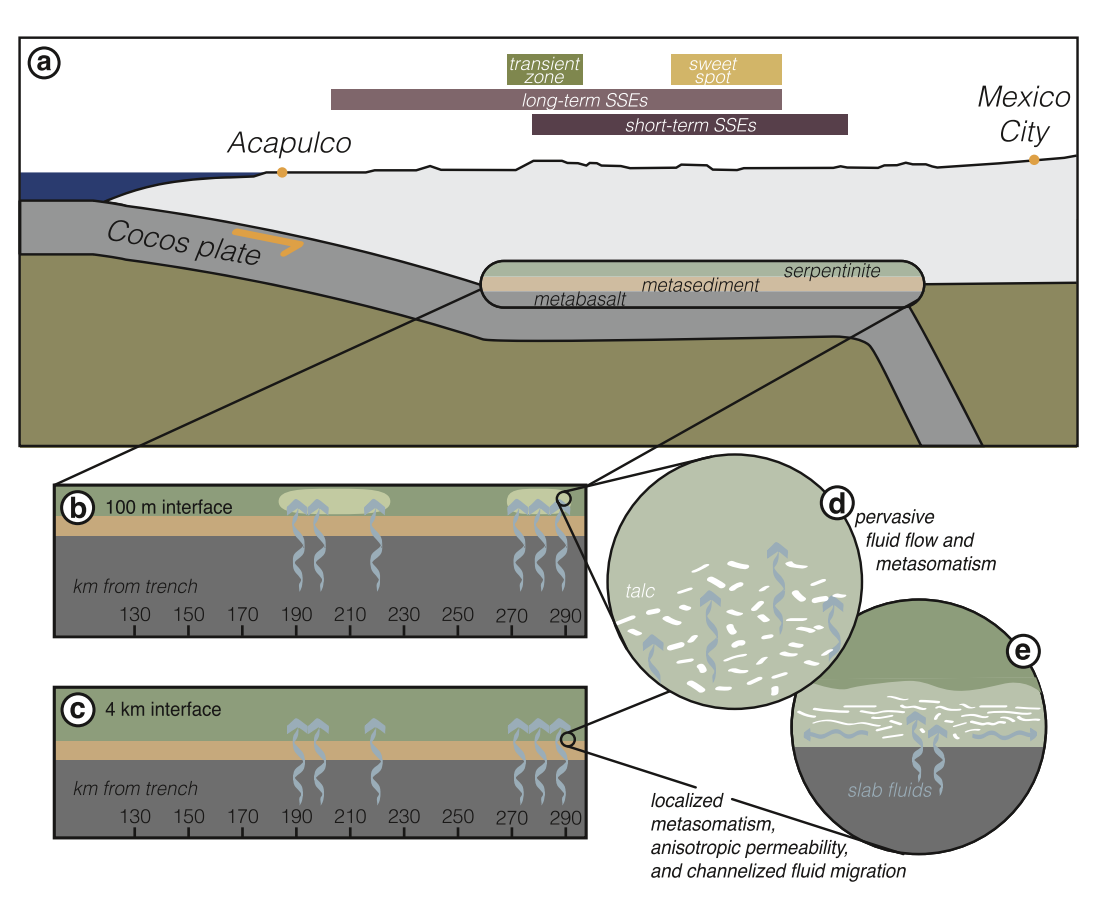


Figure 8. Schematic cross section of flat slab subduction beneath Guerrero (a) demonstrating the possible mechanisms for silica metasomatism of serpentinites at the plate interface that are explored here and comparing talc production in the (b) 100 m-thick interface and (c) 4 km-thick interface models. Blue arrows show the locations of major fluid pulses, and light green regions experience significant talc production as a result of silica metasomatism over 10 million years. The simple models of silica metasomatism considered here assume pervasive fluid flow and reaction of silica-bearing fluids with serpentinite, as in panel (d), but anisotropic permeability that develops in deformed talc-rich rocks as in panel (e) as a result of localized metasomatism that will likely occur even if the pervasive metasomatism of the whole interface is unlikely, may act to channelize fluids at the plate interface and cause the migration of silica-rich fluids to the rest of the interface where local fluid fluxes may not be high enough to promote significant talc growth, or produce pervasive talc growth as in the 4 km-thick interface.

trenchward along the plate interface from the region of the sweet spot (Frank et al., 2015a, 2015b). This migration of fluids along the plate interface may provide a mechanism for distributing silica-rich fluids from regions of high local fluid flux to regions of the flat slab with low levels of local fluid flux, and similar fluid flow patterns have been suggested by stable isotope studies from the rock record (e.g., Condit et al., 2022; Epstein et al., 2021; Jaeckel et al., 2018). The creation of talc and other phyllosilicate minerals may contribute to the production of anisotropic permeability that can help confine fluids to the plate interface region. Such impermeable barriers have been suggested as an explanation for geophysically inferred high pore-fluid pressures (e.g., Hyndman, 1988; Peacock et al., 2011), and have been suggested to channelize fluids and concentrate silica (Hyndman et al., 2015). Experiments on antigorite, on the other hand, suggest that deformed serpentinites may provide enough permeability along grain boundaries to allow fluid movement (Ganzhorn et al., 2019). The development of impermeable seals of talc schist, which are predicted by our localized metasomatism model (Figure 7), may contribute to the redistribution of fluid along the plate interface (Figure 8e), which might diminish the amount of silica introduced into the regions that experience high degrees of local silica flux and increase the silica delivery to up-dip parts of the interface that have low local silica flux.

The contrast between our 4 km-thick, 100 m-thick, and localized metasomatism models also highlights the importance of the physical pathways of fluid flow at the subduction interface, as the same volume of water released by subducting rocks may cause different degrees of metasomatism depending on the volume of serpentinite with

LINDQUIST ET AL. 18 of 23

Wiley Online Library on [09/08/2023]. See the Terms and Conditi

) on Wiley Online Library for rules of use; OA articles are governed by the applicable Creative Commons Licens

which it interacts (e.g., Figure 8d vs. Figure 8e; Figures 5a and 5b vs. Figures 5c and 5d). A thin zone of talc produced by the metasomatism of serpentinite immediately adjacent to the plate interface, as predicted in our localized metasomatism models (Figure 7), is likely rheologically signficant, as suggested by the experiments of Hirauchi et al. (2013) in which less than 10 vol. % talc was sufficient to localize frictional slip. As shown in Figure 4, the locations of pulses of high water and silica flux into the plate interface overlap with the spatial extent of SSEs, even when considering possible uncertainties in the thermal models. Talc-rich rocks are therefore likely to be present at the plate interface within some of the region that hosts slow slip—if not the entire flat plate interface—even if lateral fluid movement does not lead to a wider distribution of metasomatized rocks over the flat plate interface. No matter which process of metasomatism is dominant beneath Mexico, it is likely that a small volume of talc-bearing rocks are present along some or all of the flat plate interface and influence the slip phenomena that occur there.

The model for silica flux and talc production presented here only considers advective silica metasomatism, but other mechanisms of metasomatism may contribute to talc production in subduction zones, including mechanical mixing and diffusion. However, field-based studies of exhumed rocks from accretionary wedges and deeper in subduction zones suggest that advective silica transport can be important and externally derived fluids can transport large quantities of silica through subduction zones. For example, Breeding and Ague (2002), document extensive quartz veining in low metamorphic grade accretionary wedge rocks, indicating up to 10% increases in rock mass through quartz precipitation. Externally derived fluids have also been invoked to explain some of the vein formation and metasomatism in higher-grade mélange, metasedimentary, and metabasaltic rocks of the Catalina Schist on the basis of trace element and oxygen isotope data (Bebout, 1991; Bebout & Barton, 1993). Therefore, our results represent the effects of one, likely important, end-member mechanism for silica metasomatism and talc production at Guerrero.

7. Conclusion

We use petrologic models to explore the effects of silica metasomatism on serpentinites at the plate interface and the ability of silica advection to produce talc in these rocks above the flat slab beneath Guerrero. At the conditions of ETS beneath Guerrero, serpentinites must achieve ~43 wt. % SiO₂ to begin to stabilize talc, and ~45 wt. % SiO₂ to stabilize a rheologically significant 10 vol. % talc. Estimates of water production along the flat slab based on our petrologic models of the rocks that make up the subducting Cocos plate suggest that water and silica flux will only lead to silica metasomatism of the entire plate interface near sites of significant dehydration of metabasalts. However, localized metasomatism of serpentinite directly adjacent to the plate interface can easily produce thin zones of talc-rich rocks given the silica fluxes that we predict to occur along the entire flat slab. We also suggest that fluids are likely to migrate along the plate interface, distributing silica farther from the loci of dehydration, although silica advection by saturated aqueous fluids alone is still likely not enough to cause extensive metasomatism of the plate interface. We note, however, that other mechanisms such as mechanical mixing of more silica-rich rocks with serpentinites near the plate interface, and diffusion of silica may still lead to metasomatism and talc production. Although our estimates of talc production are not large enough to explain previous seismic velocity models of the flat plate interface beneath Mexico, our results indicate that rheologically significant volumes of talc are nonetheless likely to occur.

Conflict of Interest

The authors declare no conflicts of interest relevant to this study.

Data Availability Statement

Archives of the whole-rock data used for the petrologic modeling as well as modeling results are available in a Zenodo repository (Lindquist et al., 2023).

LINDOUIST ET AL. 19 of 23

15252027, 2023, 8, Downloaded from https://agupubs

Acknowledgments

Funding for this work was provided by NSF EAR-2119844 and Royalty Research Funds from the University of Washington awarded to C. Condit, and GSA student travel funds enabled fruitful discussion of early versions of this work at GSA 2022. We thank Whitney Behr for editorial handling and Kohtaro Ujiie and one anonymous reviewer for their constructive reviews which helped improve the quality of this manuscript.

References

- Agard, P., Plunder, A., Angiboust, S., Bonnet, G., & Ruh, J. (2018). The subduction plate interface: Rock record and mechanical coupling (from long to short timescales). *Lithos*, 320–321, 537–566. https://doi.org/10.1016/j.lithos.2018.09.029
- Angiboust, S., Pettke, T., De Hoog, J. C. M., Caron, B., & Oncken, O. (2014). Channelized fluid flow and Eclogite-facies metasomatism along the subduction shear zone. *Journal of Petrology*, 55(5), 883–916. https://doi.org/10.1093/petrology/egu010
- Bebout, G. E. (1991). Geometry and mechanisms of fluid flow at 15 to 45 kilometer depths in an early cretaceous accretionary complex. *Geophysical Research Letters*, 18(5), 923–926. https://doi.org/10.1029/91GL00949
- Bebout, G. E., & Barton, M. D. (1993). Metasomatism during subduction: Products and possible paths in the Catalina Schist, California. *Chemical Geology*, 108(1–4), 61–92, https://doi.org/10.1016/0009-2541(93)90318-D
- Bebout, G. E., & Barton, M. D. (2002). Tectonic and metasomatic mixing in a high-T, subduction-zone mélange—Insights into the geochemical evolution of the slab-mantle interface. *Chemical Geology*, 187(1), 79–106. https://doi.org/10.1016/S0009-2541(02)00019-0
- Bebout, G. E., & Penniston-Dorland, S. C. (2016). Fluid and mass transfer at subduction interfaces—The field metamorphic record. *Lithos*, 240–243, 228–258. https://doi.org/10.1016/j.lithos.2015.10.007
- Beinlich, A., John, T., Vrijmoed, J. C., Tominaga, M., Magna, T., & Podladchikov, Y. Y. (2020). Instantaneous rock transformations in the deep crust driven by reactive fluid flow. *Nature Geoscience*, 13(4), 307–311. https://doi.org/10.1038/s41561-020-0554-9
- Boneh, Y., Pec, M., & Hirth, G. (2023). High-pressure mechanical properties of talc: Implications for fault strength and slip processes. *Journal of Geophysical Research: Solid Earth*, 128(3), e2022JB025815. https://doi.org/10.1029/2022JB025815
- Boschi, C., Frueh-Green, G., & Escartin, J. (2006). Occurrence and significance of serpentinite-hosted, talc- and AMPHIBOLE-RICH fault rocks in modern oceanic settings and ophiolite complexes: An overview. Ofioliti. 31, 129–140. https://doi.org/10.4454/ofioliti.v31i2.335
- Breeding, C. M., & Ague, J. J. (2002). Slab-derived fluids and quartz-vein formation in an accretionary prism, Otago Schist, New Zealand. *Geology*, 30(6), 499–502. https://doi.org/10.1130/0091-7613(2002)030<0499:SDFAQV>2.0.CO;2
- Codillo, E. A., Klein, F., Dragovic, B., Marschall, H. R., Baxter, E., Scambelluri, M., & Schwarzenbach□, E. (2022). Fluid-mediated mass transfer between Mafic and ultramafic rocks in subduction zones. *Geochemistry, Geophysics, Geosystems*, 23(8), e2021GC010206. https://doi.org/10.1029/2021GC010206
- Codillo, E. A., Klein, F., & Marschall, H. R. (2022). Preferential formation of chlorite over talc during Si-metasomatism of ultramafic rocks in subduction zones. Geophysical Research Letters, 49(19), e2022GL100218. https://doi.org/10.1029/2022GL100218
- Collettini, C., Viti, C., Smith, S. A. F., & Holdsworth, R. E. (2009). Development of interconnected talc networks and weakening of continental low-angle normal faults. *Geology*, 37(6), 567–570. https://doi.org/10.1130/G25645A.1
- Condit, C. B., French, M. E., Hayles, J. A., Yeung, L. Y., Chin, E. J., & Lee, C.-T. A. (2022). Rheology of metasedimentary rocks at the base of
- the subduction seismogenic zone. *Geochemistry, Geophysics, Geosystems*, 23(2), e2021GC010194. https://doi.org/10.1029/2021GC010194 Condit, C. B., Guevara, V. E., Delph, J. R., & French, M. E. (2020). Slab dehydration in warm subduction zones at depths of episodic slip and
- tremor. Earth and Planetary Science Letters, 552, 116601. https://doi.org/10.1016/j.epsl.2020.116601
 Connolly, J. A. D., & Petrini, K. (2002). An automated strategy for calculation of phase diagram sections and retrieval of rock properties as a
- function of physical conditions. *Journal of Metamorphic Geology*, 20(7), 697–708. https://doi.org/10.1046/j.1525-1314.2002.00398.x Cottrell, E., & Kelley, K. A. (2011). The oxidation state of Fe in MORB glasses and the oxygen fugacity of the upper mantle. *Earth and Planetary*
- Science Letters, 305(3), 270–282. https://doi.org/10.1016/j.epsl.2011.03.014
 Cruz-Atienza, V. M., Tago, J., Villafuerte, C., Wei, M., Garza-Girón, R., Dominguez, L. A., et al. (2021). Short-term interaction between silent and devastating earthquakes in Mexico. Nature Communications. 12(1), 2171. https://doi.org/10.1038/s41467-021-22326-6
- DeMets, C., Gordon, R. G., & Argus, D. F. (2010). Geologically current plate motions. *Geophysical Journal International*, 181(1), 1–80. https://doi.org/10.1111/j.1365-246X.2009.04491.x
- Deschamps, F., Godard, M., Guillot, S., & Hattori, K. (2013). Geochemistry of subduction zone serpentinites: A review. *Lithos*, 178, 96–127. https://doi.org/10.1016/j.lithos.2013.05.019
- Epstein, G. S., Bebout, G. E., & Angiboust, S. (2021). Fluid and mass transfer along transient subduction interfaces in a deep paleo-accretionary wedge (Western Alps). Chemical Geology, 559, 119920. https://doi.org/10.1016/j.chemgeo.2020.119920
- Escartín, J., Andreani, M., Hirth, G., & Evans, B. (2008). Relationships between the microstructural evolution and the rheology of talc at elevated pressures and temperatures. *Earth and Planetary Science Letters*, 268(3), 463–475. https://doi.org/10.1016/j.epsl.2008.02.004
- Evans, B. W. (2008). Control of the products of serpentinization by the Fe²⁺Mg₋₁ exchange potential of olivine and orthopyroxene. *Journal of Petrology*, 49(10), 1873–1887. https://doi.org/10.1093/petrology/egn050
- Ferrari, L., Orozco-Esquivel, T., Manea, V., & Manea, M. (2012). The dynamic history of the Trans-Mexican Volcanic Belt and the Mexico subduction zone. *Tectonophysics*. 522–523. 122–149. https://doi.org/10.1016/j.tecto.2011.09.018
- Forshaw, J. B., & Pattison, D. R. M. (2021). Ferrous/ferric (Fe²⁺/Fe³⁺) partitioning among silicates in metapelites. *Contributions to Mineralogy and Petrology*, 176(9), 63, https://doi.org/10.1007/s00410-021-01814-4
- Frank, W. B., Radiguet, M., Rousset, B., Shapiro, N. M., Husker, A. L., Kostoglodov, V., et al. (2015a). Uncovering the geodetic signature of silent slip through repeating earthquakes. *Geophysical Research Letters*, 42(8), 2774–2779. https://doi.org/10.1002/2015GL063685
- Frank, W. B., Shapiro, N. M., Husker, A. L., Kostoglodov, V., Bhat, H. S., & Campillo, M. (2015b). Along-fault pore-pressure evolution during a slow-slip event in Guerrero, Mexico. Earth and Planetary Science Letters, 413, 135–143. https://doi.org/10.1016/j.epsl.2014.12.051
- Frank, W. B., Shapiro, N. M., Husker, A. L., Kostoglodov, V., Romanenko, A., & Campillo, M. (2014). Using systematically characterized low-frequency earthquakes as a fault probe in Guerrero, Mexico. *Journal of Geophysical Research: Solid Earth*, 119(10), 7686–7700. https://doi.org/10.1002/2014JB011457
- French, M. E., & Condit, C. B. (2019). Slip partitioning along an idealized subduction plate boundary at deep slow slip conditions. *Earth and Planetary Science Letters*, 528, 115828. https://doi.org/10.1016/j.epsl.2019.115828
- Gale, A., Dalton, C. A., Langmuir, C. H., Su, Y., & Schilling, J.-G. (2013). The mean composition of ocean ridge basalts. *Geochemistry, Geophysics, Geosystems*, 14(3), 489–518. https://doi.org/10.1029/2012GC004334
- Ganzhorn, A. C., Pilorgé, H., & Reynard, B. (2019). Porosity of metamorphic rocks and fluid migration within subduction interfaces. *Earth and Planetary Science Letters*, 522, 107–117. https://doi.org/10.1016/j.epsl.2019.06.030
- Gervais, F., & Trapy, P.-H. (2021). Testing solution models for phase equilibrium (forward) modeling of partial melting experiments. *Contributions to Mineralogy and Petrology*, 176(1), 4. https://doi.org/10.1007/s00410-020-01762-5
- Gutiérrez-Aguilar, F., Hernández-Uribe, D., Holder, R. M., & Condit, C. B. (2022). Fluid-Induced fault reactivation due to Brucite + antigorite dehydration triggered the Mw7.1 September 19th Puebla-Morelos (Mexico) intermediate-depth earthquake. *Geophysical Research Letters*, 49(20), e2022GL100814. https://doi.org/10.1029/2022GL100814

LINDOUIST ET AL. 20 of 23

- Gyomlai, T., Agard, P., Marschall, H. R., Jolivet, L., & Gerdes, A. (2021). Metasomatism and deformation of block-in-matrix structures in Syros: The role of inheritance and fluid-rock interactions along the subduction interface. *Lithos*, 386–387, 105996. https://doi.org/10.1016/j. lithos.2021.105996
- Hayes, G. P., Moore, G. L., Portner, D. E., Hearne, M., Flamme, H., Furtney, M., & Smoczyk, G. M. (2018). Slab2, a comprehensive subduction zone geometry model. *Science*, 362(6410), 58–61. https://doi.org/10.1126/science.aat4723
- Hernández-Uribe, D., & Palin, R. M. (2019). A revised petrological model for subducted oceanic crust: Insights from phase equilibrium modelling. *Journal of Metamorphic Geology*, 37(6), 745–768. https://doi.org/10.1111/jmg.12483
- Hernández-Uribe, D., Palin, R. M., Cone, K. A., & Cao, W. (2020). Petrological implications of seafloor hydrothermal alteration of subducted mid-ocean ridge basalt. *Journal of Petrology*, 61(9), egaa086. https://doi.org/10.1093/petrology/egaa086
- Hirauchi, K., den Hartog, S. A. M., & Spiers, C. J. (2013). Weakening of the slab—mantle wedge interface induced by metasomatic growth of talc. *Geology*, 41(1), 75–78. https://doi.org/10.1130/G33552.1
- Hirauchi, K., Yamamoto, Y., den Hartog, S. A. M., & Niemeijer, A. R. (2020). The role of metasomatic alteration on frictional properties of subduction thrusts: An example from a serpentinite body in the Franciscan Complex, California. Earth and Planetary Science Letters, 531, 115967. https://doi.org/10.1016/j.epsl.2019.115967
- Holland, T. J. B., & Powell, R. (1991). A Compensated-Redlich-Kwong (CORK) equation for volumes and fugacities of CO₂ and H₂O in the range 1 bar to 50 kbar and 100–1600°C. Contributions to Mineralogy and Petrology, 109(2), 265–273. https://doi.org/10.1007/BF00306484
- Holland, T. J. B., & Powell, R. (1998). An internally consistent thermodynamic data set for phases of petrological interest. *Journal of Metamor-phic Geology*, 16(3), 309–343. https://doi.org/10.1111/j.1525-1314.1998.00140.x
- Holland, T. J. B., & Powell, R. (2011). An improved and extended internally consistent thermodynamic dataset for phases of petrological interest, involving a new equation of state for solids. *Journal of Metamorphic Geology*, 29(3), 333–383. https://doi.org/10.1111/j.1525-1314.2010.00923.x
- Hoover, W. F., Condit, C. B., Lindquist, P. C., Moser, A. C., & Guevara, V. E. (2022). Episodic slow slip hosted by talc-bearing metasomatic rocks: High strain rates and stress amplification in a chemically reacting shear zone. Geophysical Research Letters, 49(21), e2022GL101083. https://doi.org/10.1029/2022GL101083
- Husker, A. L., Kostoglodov, V., Cruz-Atienza, V. M., Legrand, D., Shapiro, N. M., Payero, J. S., et al. (2012). Temporal variations of non-volcanic tremor (NVT) locations in the Mexican subduction zone: Finding the NVT sweet spot. Geochemistry, Geophysics, Geosystems, 13(3). https://doi.org/10.1029/2011GC003916
- Hyndman, R. D. (1988). Dipping seismic reflectors, electrically conductive zones, and trapped water in the crust over a subducting plate. *Journal of Geophysical Research*, 93(B11), 13391–13405. https://doi.org/10.1029/JB093iB11p13391
- Hyndman, R. D., McCrory, P. A., Wech, A., Kao, H., & Ague, J. (2015). Cascadia subducting plate fluids channelled to fore-arc mantle corner: ETS and silica deposition. *Journal of Geophysical Research: Solid Earth*, 120(6), 4344–4358. https://doi.org/10.1002/2015JB011920
- Jaeckel, K., Bebout, G. E., & Angiboust, S. (2018). Deformation-enhanced fluid and mass transfer along Western and Central Alps paleo-subduction interfaces: Significance for carbon cycling models. Geosphere, 14(6), 2355–2375. https://doi.org/10.1130/GES01587.1
- Jarrard, R. D. (2003). Subduction fluxes of water, carbon dioxide, chlorine, and potassium. *Geochemistry, Geophysics, Geosystems*, 4(5), 8905. https://doi.org/10.1029/2002GC000392
- Joron, J. L., Bougault, H., Maury, R. C., & Stephan, J. F. (1982). Basalt from the Cocos plate, Site 487, Leg 66: Petrology and Geochemistry. Deep Sea Drilling Project Reports and Publications No. 66 (pp. 731–734). https://doi.org/10.2973/dsdp.proc.66.136.1982
- Kerrick, D. M., & Connolly, J. A. D. (2001). Metamorphic devolatilization of subducted oceanic metabasalts: Implications for seismicity, arc magmatism and volatile recycling. Earth and Planetary Science Letters, 189(1), 19–29. https://doi.org/10.1016/S0012-821X(01)00347-8
- Kim, Y., Clayton, R. W., & Jackson, J. M. (2010). Geometry and seismic properties of the subducting Cocos plate in central Mexico. *Journal of Geophysical Research*, 115(B6), B06310. https://doi.org/10.1029/2009JB006942
- Kostoglodov, V., Husker, A., Shapiro, N. M., Payero, J. S., Campillo, M., Cotte, N., & Clayton, R. (2010). The 2006 slow slip event and nonvolcanic tremor in the Mexican subduction zone. *Geophysical Research Letters*, 37(24), L24301. https://doi.org/10.1029/2010GL045424
- Kostoglodov, V., Singh, S. K., Santiago, J. A., Franco, S. I., Larson, K. M., Lowry, A. R., & Bilham, R. (2003). A large silent earthquake in the Guerrero seismic gap, Mexico. *Geophysical Research Letters*, 30(15), 1807. https://doi.org/10.1029/2003GL017219
- Lindquist, P., Condit, C., Hoover, W., Guevara, V., & Hernández Uribe, D. (2023). Data for Lindquist et al., metasomatism and slow slip: Talc production along the flat subduction plate interface beneath Mexico (Guerrero) [Dataset]. Zenodo. https://doi.org/10.5281/zenodo.8034024
- Lowry, A. R., Larson, K. M., Kostoglodov, V., & Bilham, R. (2001). Transient fault slip in Guerrero, southern Mexico. Geophysical Research Letters, 28(19), 3753–3756. https://doi.org/10.1029/2001GL013238
- Manea, V. C., & Manea, M. (2011). Flat-slab thermal structure and evolution beneath Central Mexico. *Pure and Applied Geophysics*, 168(8), 1475–1487. https://doi.org/10.1007/s00024-010-0207-9
- Manea, V. C., Manea, M., & Ferrari, L. (2013). A geodynamical perspective on the subduction of Cocos and Rivera plates beneath Mexico and Central America. *Tectonophysics*, 609, 56–81. https://doi.org/10.1016/j.tecto.2012.12.039
- Manea, V. C., Manea, M., Kostoglodov, V., Currie, C. A., & Sewell, G. (2004). Thermal structure, coupling and metamorphism in the Mexican subduction zone beneath Guerrero. Geophysical Journal International, 158(2), 775–784. https://doi.org/10.1111/j.1365-246X.2004.02325.x
- Manning, C. E. (1994). The solubility of quartz in H2O in the lower crust and upper mantle. *Geochimica et Cosmochimica Acta*, 58(22), 4831–4839. https://doi.org/10.1016/0016-7037(94)90214-3
- Manning, C. E. (1995). Phase-equilibrium controls on SiO₂ metasomatism by aqueous fluid in subduction zones: Reaction at constant pressure and temperature. *International Geology Review*, 37(12), 1074–1093. https://doi.org/10.1080/00206819509465440
- Manning, C. E. (1997). Coupled reaction and flow in subduction zones: Silica metasomatism in the mantle wedge. Fluid Flow and Transport in Rocks: Mechanisms and Effects, 139–148.
- Manning, C. E. (2004). The chemistry of subduction-zone fluids. Earth and Planetary Science Letters, 223(1), 1–16. https://doi.org/10.1016/j.
- Misra, S., Boutareaud, S., & Burg, J.-P. (2014). Rheology of talc sheared at high pressure and temperature: A case study for hot subduction zones. Tectonophysics, 610, 51–62. https://doi.org/10.1016/j.tecto.2013.10.009
- Moore, D. E., & Lockner, D. A. (2008). Talc friction in the temperature range 25°-400°C: Relevance for fault-zone weakening. *Tectonophysics*, 449(1), 120–132. https://doi.org/10.1016/j.tecto.2007.11.039
- Moore, D. E., & Rymer, M. J. (2007). Talc-bearing serpentinite and the creeping section of the San Andreas fault. *Nature*, 448(7155), 795–797. https://doi.org/10.1038/nature06064
- Naif, S., Key, K., Constable, S., & Evans, R. L. (2015). Water-rich bending faults at the Middle America Trench. Geochemistry, Geophysics, Geosystems, 16(8), 2582–2597. https://doi.org/10.1002/2015GC005927
- Nishiyama, N., Ujiie, K., Noro, K., Mori, Y., & Masuyama, H. (2023). Megathrust slip enhanced by metasomatic actinolite in the source region of deep slow slip. Lithos, 446–447, 107115. https://doi.org/10.1016/j.lithos.2023.107115

LINDOUIST ET AL. 21 of 23

5252027, 2023, 8, Downloaded from https://agupubs

- Okamoto, A., Oyanagi, R., Yoshida, K., Uno, M., Shimizu, H., & Satish-Kumar, M. (2021). Rupture of wet mantle wedge by self-promoting carbonation. *Communications Earth & Environment*, 2(1), 1–10. https://doi.org/10.1038/s43247-021-00224-5
- Palin, R. M., Weller, O. M., Waters, D. J., & Dyck, B. (2016). Quantifying geological uncertainty in metamorphic phase equilibria model-ling; a Monte Carlo assessment and implications for tectonic interpretations. Geoscience Frontiers, 7(4), 591–607. https://doi.org/10.1016/j.gsf.2015.08.005
- Pawley, A. R., & Wood, B. J. (1995). The high-pressure stability of talc and 10 Å phase: Potential storage sites for H₂O in subduction zones. American Mineralogist, 80(9–10), 998–1003. https://doi.org/10.2138/am-1995-9-1015
- Peacock, S. M. (2009). Thermal and metamorphic environment of subduction zone episodic tremor and slip. *Journal of Geophysical Research*, 114(B8), B00A07. https://doi.org/10.1029/2008JB005978
- Peacock, S. M., Christensen, N. I., Bostock, M. G., & Audet, P. (2011). High pore pressures and porosity at 35 km depth in the Cascadia subduction zone. *Geology*, 39(5), 471–474. https://doi.org/10.1130/G31649.1
- Peacock, S. M., & Hyndman, R. D. (1999). Hydrous minerals in the mantle wedge and the maximum depth of subduction thrust earthquakes. Geophysical Research Letters, 26(16), 2517–2520. https://doi.org/10.1029/1999GL900558
- Peacock, S. M., & Wang, K. (2021). On the stability of talc in subduction zones: A possible control on the maximum depth of decoupling between the subducting plate and mantle wedge. *Geophysical Research Letters*, 48(17), e2021GL094889. https://doi.org/10.1029/2021GL094889
- Penniston-Dorland, S. C., Gorman, J. K., Bebout, G. E., Piccoli, P. M., & Walker, R. J. (2014). Reaction rind formation in the Catalina Schist: Deciphering a history of mechanical mixing and metasomatic alteration. *Chemical Geology*, 384, 47–61. https://doi.org/10.1016/j. chemgeo.2014.06.024
- Pérez-Campos, X., Kim, Y., Husker, A., Davis, P. M., Clayton, R. W., Iglesias, A., et al. (2008). Horizontal subduction and truncation of the Cocos plate beneath central Mexico. *Geophysical Research Letters*, 35(18), L18303. https://doi.org/10.1029/2008GL035127
- Perez-Silva, A., Li, D., Gabriel, A.-A., & Kaneko, Y. (2021). 3D modeling of long-term slow slip events along the flat-slab segment in the Guerrero seismic gap, Mexico. Geophysical Research Letters, 48(13), e2021GL092968. https://doi.org/10.1029/2021GL092968
- Perry, M., Spinelli, G. A., Wada, I., & He, J. (2016). Modeled temperatures and fluid source distributions for the Mexican subduction zone: Effects of hydrothermal circulation and implications for plate boundary seismic processes. *Geochemistry, Geophysics, Geosystems*, 17(2), 550–570. https://doi.org/10.1002/2015GC006148
- Pitzer, K. S., & Sterner, S. M. (1994). Equations of state valid continuously from zero to extreme pressures for H₂O and CO₂. The Journal of Chemical Physics, 101(4), 3111–3116. https://doi.org/10.1063/1.467624
- Plank, T., & Langmuir, C. H. (1998). The chemical composition of subducting sediment and its consequences for the crust and mantle. Chemical Geology, 145(3), 325–394. https://doi.org/10.1016/S0009-2541(97)00150-2
- Powell, R., & Holland, T. J. B. (2008). On thermobarometry. *Journal of Metamorphic Geology*, 26(2), 155–179. https://doi. org/10.1111/j.1525-1314.2007.00756.x
- Radiguet, M., Cotton, F., Vergnolle, M., Campillo, M., Walpersdorf, A., Cotte, N., & Kostoglodov, V. (2012). Slow slip events and strain accumulation in the Guerrero gap, Mexico. *Journal of Geophysical Research*, 117(B4), B04305. https://doi.org/10.1029/2011JB008801
- Rüpke, L. H., Morgan, J. P., Hort, M., & Connolly, J. A. D. (2004). Serpentine and the subduction zone water cycle. Earth and Planetary Science Letters, 223(1), 17–34. https://doi.org/10.1016/j.epsl.2004.04.018
- Sdrolias, M., & Müller, R. D. (2006). Controls on back-arc basin formation. Geochemistry, Geophysics, Geosystems, 7(4), Q04016. https://doi.org/10.1029/2005GC001090
- Sieber, M. J., Yaxley, G. M., & Hermann, J. (2022). COH-fluid induced metasomatism of peridotites in the forearc mantle. *Contributions to Mineralogy and Petrology*, 177(4), 44. https://doi.org/10.1007/s00410-022-01905-w
- Song, T.-R. A., Helmberger, D. V., Brudzinski, M. R., Clayton, R. W., Davis, P., Pérez-Campos, X., & Singh, S. K. (2009). Subducting slab ultra-slow velocity layer coincident with silent earthquakes in southern Mexico. *Science*, 324(5926), 502–506. https://doi.org/10.1126/science.1167595
- Song, T.-R. A., & Kim, Y. (2012). Localized seismic anisotropy associated with long-term slow-slip events beneath southern Mexico. Geophysical Research Letters, 39(9), L09308. https://doi.org/10.1029/2012GL051324
- Spandler, C., Hermann, J., Faure, K., Mavrogenes, J. A., & Arculus, R. J. (2008). The importance of talc and chlorite "hybrid" rocks for volatile recycling through subduction zones; evidence from the high-pressure subduction mélange of New Caledonia. Contributions to Mineralogy and Petrology, 155(2), 181–198. https://doi.org/10.1007/s00410-007-0236-2
- Syracuse, E. M., van Keken, P. E., & Abers, G. A. (2010). The global range of subduction zone thermal models. *Physics of the Earth and Planetary Interiors*, 183(1), 73–90. https://doi.org/10.1016/j.pepi.2010.02.004
- Tarling, M. S., Smith, S. A. F., & Scott, J. M. (2019). Fluid overpressure from chemical reactions in serpentinite within the source region of deep episodic tremor. *Nature Geoscience*, 12(12), 1034–1042. https://doi.org/10.1038/s41561-019-0470-z
- Ujiie, K., Noro, K., Shigematsu, N., Fagereng, Å., Nishiyama, N., Tulley, C. J., et al. (2022). Megathrust shear modulated by Albite metasomatism in subduction mélanges. *Geochemistry, Geophysics, Geosystems*, 23(8), e2022GC010569. https://doi.org/10.1029/2022GC010569
- van Keken, P. E., Wada, I., Abers, G. A., Hacker, B. R., & Wang, K. (2018). Mafic high-pressure rocks are preferentially exhumed from warm subduction settings. *Geochemistry, Geophysics, Geosystems*, 19(9), 2934–2961. https://doi.org/10.1029/2018GC007624
- Villafuerte, C., & Cruz-Atienza, V. M. (2017). Insights into the causal relationship between slow slip and tectonic tremor in Guerrero, Mexico. Journal of Geophysical Research: Solid Earth, 122(8), 6642–6656. https://doi.org/10.1002/2017JB014037
- Watkins, J. S., Moore, J. C., Bachman, S. B., Behtel, F. W., Didyk, B. M., Leggett, J. K., et al. (1982). Site 487 (Initial Reports of the Deep Sea Drilling Project No. Volume 66). https://doi.org/10.2973/dsdp.proc.66.103.1982
- Whitney, D. L., & Evans, B. W. (2010). Abbreviations for names of rock-forming minerals. *American Mineralogist*, 95(1), 185–187. https://doi.org/10.2138/am.2010.3371

References From the Supporting Information

- Diener, J. F. A., & Powell, R. (2012). Revised activity–composition models for clinopyroxene and amphibole. *Journal of Metamorphic Geology*, 30(2), 131–142. https://doi.org/10.1111/j.1525-1314.2011.00959.x
- Fuhrman, M. L., & Lindsley, D. H. (1988). Ternary-feldspar modeling and thermometry. American Mineralogist, 73(3-4), 201-215.
- Green, E., Holland, T., & Powell, R. (2007). An order-disorder model for omphacitic pyroxenes in the system jadeite-diopside-hedenbergite-acmite, with applications to eclogitic rocks. *American Mineralogist*, 92(7), 1181–1189. https://doi.org/10.2138/am.2007.2401
- Green, E. C. R., White, R. W., Diener, J. F. A., Powell, R., Holland, T. J. B., & Palin, R. M. (2016). Activity–composition relations for the calculation of partial melting equilibria in metabasic rocks. *Journal of Metamorphic Geology*, 34(9), 845–869. https://doi.org/10.1111/jmg.12211

LINDOUIST ET AL. 22 of 23



Geochemistry, Geophysics, Geosystems

- 10.1029/2023GC010981
- Massonne, H.-J., & Willner, A. P. (2008). Phase relations and dehydration behaviour of psammopelite and mid-ocean ridge basalt at very-low-grade to low-grade metamorphic conditions. *European Journal of Mineralogy*, 20(5), 867–879. https://doi.org/10.1127/0935-1221/2008/0020-1871
- Padrón-Navarta, J. A., Sánchez-Vizcaíno, V. L., Hermann, J., Connolly, J. A. D., Garrido, C. J., Gómez-Pugnaire, M. T., & Marchesi, C. (2013). Tschermak's substitution in antigorite and consequences for phase relations and water liberation in high-grade serpentinites. *Lithos*, 178, 186–196. https://doi.org/10.1016/j.lithos.2013.02.001
- Powell, R., & Holland, T. (1999). Relating formulations of the thermodynamics of mineral solid solutions; activity modeling of pyroxenes, amphiboles, and micas. *American Mineralogist*, 84(1–2), 1–14. https://doi.org/10.2138/am-1999-1-201
- White, P., Worley, H., Holland, & Worley (2000). The effect of TiO₂ and Fe₂O₃ on metapelitic assemblages at greenschist and amphibolite facies conditions: Mineral equilibria calculations in the system K₂O–FeO–MgO–Al₂O₃–SiO₂–H₂O–TiO₂–Fe₂O₃. *Journal of Metamorphic Geology*, 18(5), 497–511. https://doi.org/10.1046/j.1525-1314.2000.00269.x
- White, R. W., Powell, R., & Clarke, G. L. (2002). The interpretation of reaction textures in Fe-rich metapelitic granulites of the Musgrave block, central Australia: Constraints from mineral equilibria calculations in the system K₂O–FeO–MgO–Al₂O₃–SiO₂–H₂O–TiO₂–Fe₂O₃. *Journal of Metamorphic Geology*, 20(1), 41–55. https://doi.org/10.1046/j.0263-4929.2001.00349.x
- White, R. W., Powell, R., & Holland, T. J. B. (2007). Progress relating to calculation of partial melting equilibria for metapelites. *Journal of Metamorphic Geology*, 25(5), 511–527. https://doi.org/10.1111/j.1525-1314.2007.00711.x
- White, R. W., Powell, R., Holland, T. J. B., Johnson, T. E., & Green, E. C. R. (2014a). New mineral activity-composition relations for thermodynamic calculations in metapelitic systems. *Journal of Metamorphic Geology*, 32(3), 261–286. https://doi.org/10.1111/jmg.12071
- White, R. W., Powell, R., & Johnson, T. E. (2014b). The effect of Mn on mineral stability in metapelites revisited: New a–x relations for manganese-bearing minerals. *Journal of Metamorphic Geology*, 32(8), 809–828. https://doi.org/10.1111/jmg.12095

LINDQUIST ET AL. 23 of 23